1 Metallocenium Salts of Radical Anion Bis(Dichalcogenate) Metalates

*Vasco Pires Silva da Gama and Maria Teresa Duarté*

1.1 Introduction

For the last 30 years metal-bis(1,2-dichalcogenate) anionic complexes have been extensively used as building blocks for the preparation of both conducting and magnetic molecular materials. Several of these materials show remarkable features and have made a significant contribution to the development of molecular materials science.

It is worth mentioning some examples of the molecular materials based on metal-bis(1,2-dichalcogenate) anionic complexes based that have made a significant contribution to the field of molecular material science, in the last decades. A large number of molecular conductors and even superconductors based on metal-bis(1,2-dichalcogenate) anionic acceptors have been obtained [1] and $Me_4N[Ni(dmit)_2]_2$ (dmit = 1,3-dithiol-2-thione-4,5-dithiolate) was the first example of a π acceptor superconductor with a closed-shell donor [2]. The spin-Peierls transition was observed for the first time in the linear spin chain system $TTF[Cu(tdt)_2]$ [3] (TTF = tetrathiafulvalene; tdt = 1,2-ditrifluoromethyl-1,2-ethylenedithioate). The co-existence of linear spin chains and conducting electrons, was observed for the first time in the compounds $Per_2[M(mnt)_2]$ (M = Ni, Pd, Pt) [4] (mnt = 1,2-dicyano-1,2-ethylene-dithiolato), presenting competing spin-Peierls and Peierls instabilities of the spin chains and 1D conducting electronic systems. A purely organic system with a spin-ladder configuration was observed for the first time in the compound $DT-TTF_2[Au(mnt)_2]$ [5] (DT-TTF = dithiophentetrathiafulvalene). A spin transition was observed in the compound $[Fe(mnt)_2rad]$ [6], where rad = 2-(p-N-methylpyridinium)4,4,5,5-tetramethylimidazoline-1-oxyl. Ferromagnetic ordering was reported for $NH_4[Ni(mnt)_2]H_2O$ [7].

The discovery of the first molecule-based material exhibiting ferromagnetic ordering, the electron-transfer (ET) salt $[Fe(Cp^*)_2]TCNE$ (TCNE = tetracyanoethylene), with $T_C = 4.8$ K, in 1986 [8, 9], was a landmark in molecular magnetism and gave a significant impulse to this field. Since then among the strategies followed to obtain cooperative magnetic properties, considerable attention has been given to the linear-chain electron-transfer salts based on metallocenium donors and on planar acceptors. [10, 11]. Besides $[Fe(Cp^*)_2]TCNE$, bulk ferromagnetism was reported
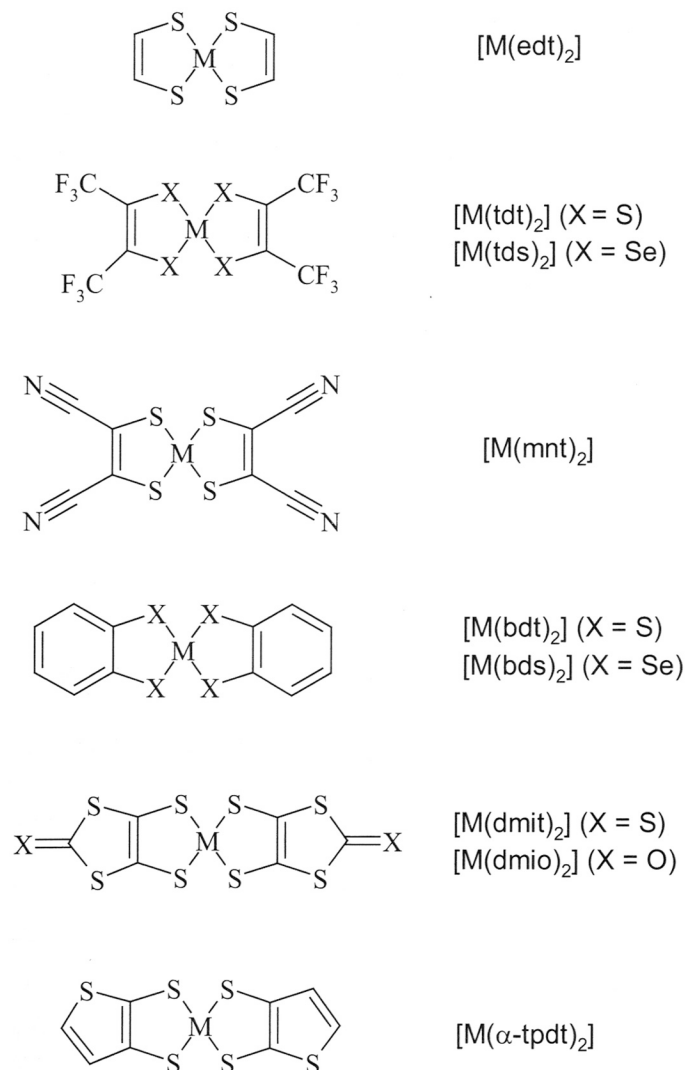
for other ET salts based on decamethylmetallocenes and on the conjugated polyni-
triles TCNE [12] and TCNQ [13] (TCNQ = 7,7,8,8-tetracyano-p-quinodimethane).
An extensive study of these salts was made, covering a variety of aspects including
the structure-magnetic property relationship [10], and the effects of spin variation
and of spinless defects [10]. Furthermore they provided a valuable basis to test the
various models that were proposed in order to explain the magnetic coupling and
magnetic ordering in the molecule-based magnets [14, 15].
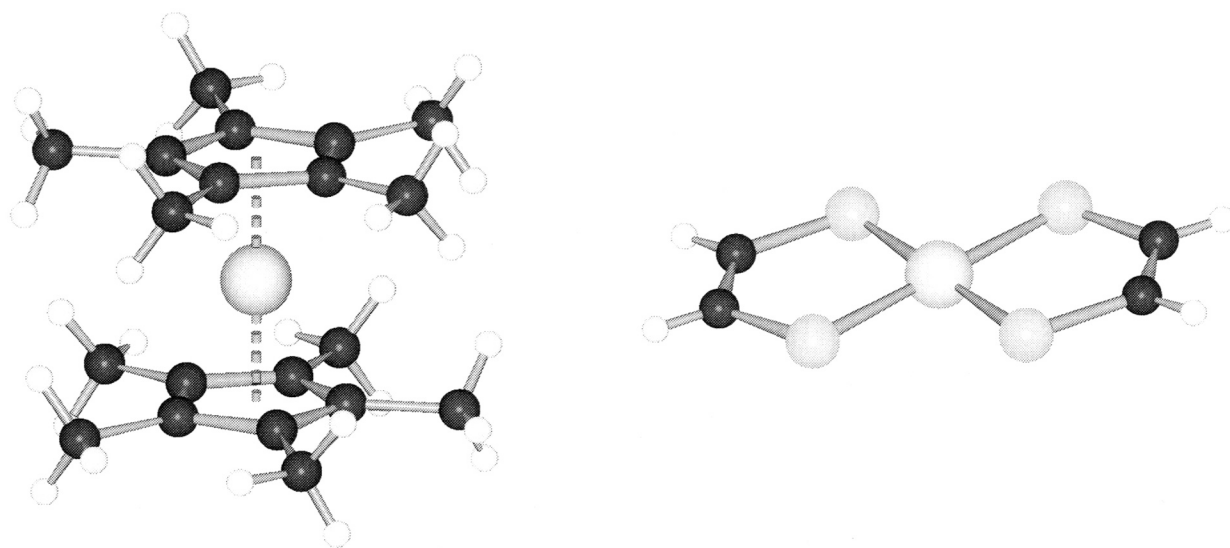
Fig. 1.1. Molecular structure of [Fe(Cp*)$_2$][Ni(edt)$_2$], showing the basic donor and acceptor
molecules studied in this review.

Following the report of ferromagnetism for [Fe(Cp*)$_2$]TCNE, metal bis-
dichalcogenate planar acceptors were also considered as suitable candidates for
use in the preparation of ET salts with the radical metallocenium donors, and in
the search for new molecular magnets the first metal bis-dichalcogenate based
compounds were reported in 1989 [16, 17]. In particular the monoanionic forms
of the metal bis-dichalcogenate (Ni, Pd, Pt) complexes seem particularly promis-
ing for "the synthesis of mixed-stack molecular charge-transfer salts that dis-
play cooperative magnetic phenomena due to (1) their planar structures, (2) de-
localized electronic states, $S = 1/2$ spin state for the monomeric species, and
(3) the possibility of extended magnetic interactions mediated by the chalcogen
atoms" [17].

The work with ET salts based on metallocenium donors and on planar metal bis-
dichalcogenate radical anions is summarized in this chapter. Most of the materials
studied to date are decamethylmetallocenium based ET salts, other compounds
based on different metallocenium derivatives have also been reported and will be

[M(edt)$_2$]

[M(tdt)$_2$] (X = S)
[M(tds)$_2$] (X = Se)

[M(mnt)$_2$]

[M(bdt)$_2$] (X = S)
[M(bds)$_2$] (X = Se)

[M(dmit)$_2$] (X = S)
[M(dmio)$_2$] (X = O)

[M(α-tpdt)$_2$]

**Scheme 1.1** Schematic representation of the metal bis-dichalcogenate acceptors studied in this chapter.

referred to. The metal bis-dichalcogenate complexes mentioned in this chapter are represented in Scheme 1.1.

As magnetic ordering is a bulk property, particular attention will be given to the supramolecular arrangements which determine the magnetic behavior. The crystal structure of the compounds will be correlated with the magnetic behavior of these ET salts. The magnetic coupling in the ET salts based on decamethylmetallocenium donors has been analyzed mainly through McConnell I [18] or McConnell II [19] mechanisms, and this issue is still a subject of controversy [15, 20]. Of these models, McConnell I has been most often used in the interpretation of the magnetic behavior of these salts, as, in spite of its simplicity, it has shown good agreement with the experimental observations. In this chapter the interpretation of the magnetic coupling will be analyzed in the perspective of this model. However, it should be mentioned that the validity of the McConnell I mechanism has been questioned both theoretically [21] and experimentally [22].

1.2   Basic Structural Motifs

1.2.1   ET Salts Based on Decamethylmetallocenium Donors

In most of the ET salts based on decamethylmetallocenium donors, due to the planar configurations of both the C_5Me_5 ligands and of the metal bis-dichalcogenate acceptors the crystal structures are, with a few exceptions, based on linear chain arrangements of alternating donor and acceptor molecules. In these salts four distinct types of linear chain arrangements have been observed and are represented schematically in Figure 1.2. The type I chain arrangement corresponds to the most simple case of an alternated linear chain motif $\cdot\cdot A^-D^+A^-D^+A^-D^+\cdot\cdot$, similar to that observed in several salts based on metallocenium donors and on acceptors such as TCNE and TCNQ [10]. In the case of the type II chain, the donors alternate with face-to-face pairs of acceptors, $\cdot\cdot A^-A^-D^+A^-A^-D^+\cdot\cdot$, as in this arrangement there is a net charge $(-)$ per repeat unit, $A^-A^-D^+$, charge compensation is required. For the type III arrangement the linear chains consist of alternated face-to-face pairs of acceptors with side-by-side pairs of donors, $\cdot\cdot A^-A^-D^+D^+A^-A^-D^+D^+\cdot\cdot$. Finally in the type IV arrangement, the acceptors alternate with side-by-side pairs of donors, $\cdot\cdot A^-D^+D^+A^-D^+D^+\cdot\cdot$, in this case there is a net charge $(+)$ per repeat unit, $D^+D^+A^-$, which must be compensated. For most of the ET salts based on types I and III arrangements (neutral chains), only one type of chain arrangement was observed. However, in the case of compounds based on types II and IV arrangements (charged chains), more complex crystal structures could be observed, resulting from the required charge neutralization. Table 1.1 summarizes the unit cell parameters, space group symmetry, and the type of observed linear chain ar-

I   II   III   IV
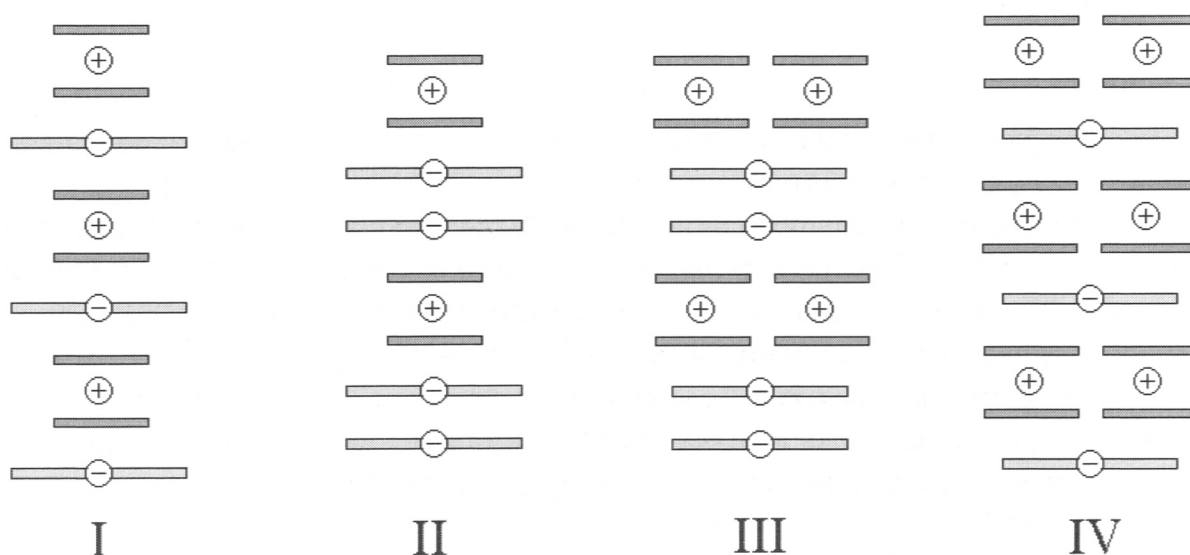
Fig. 1.2. Representation of the basic types of mixed chain sequences observed in the ET salts based on metallocene donors and on metal bis-dichalcogenate acceptors.

Table 1.1. Unit cell parameters and chain type for the mixed chain salts.

Compound	Chain Type	Space Group	a, Å	b, Å	c, Å	α, °	β, °	γ, °	Vol., Å^3	Z	T, °C	Ref.
[Fe(Cp*)$_2$][Ni(edt)$_2$]	I	C2/m	13.319	13.699	8.719	90.00	125.06	90.00	1302	2	20	23
[Cr(Cp*)$_2$][Ni(edt)$_2$]	I	C2/m	13.44	13.66	8.96	90.0	124.2	90.0	1320	2	20	23
[Fe(Cp*)$_2$][Ni(tdt)$_2$]	I	C2/c	14.417	12.659	18.454	90.00	95.17	90.00	3354	4	-70	16
[Mn(Cp*)$_2$][Ni(tdt)$_2$]	I	C2/c	14.302	12.697	18.415	90.00	94.63	90.00	3333	4	(a)	24
[Fe(Cp*)$_2$][Pt(tdt)$_2$]	I	$P\bar{1}$	8.490	10.278	10.936	106.79	103.95	101.98	846	1	-70	25
[Fe(Cp*)$_2$][Ni(tds)$_2$]	I	$P\bar{1}$	8.581	10.464	11.132	107.96	103.65	101.82	881	1	20	26
[Mn(Cp*)$_2$][Ni(tds)$_2$]	I	$P\bar{1}$	8.582	10.472	11.158	108.41	103.57	101.79	882	1	20	27
[Cr(Cp*)$_2$][Ni(tds)$_2$]	I	$P\bar{1}$	8.580	10.547	11.138	109.49	103.20	101.76	881	1	20	28
[Fe(Cp*)$_2$][Pt(tds)$_2$]	I	$P\bar{1}$	8.606	10.521	11.138	108.81	102.89	101.30	891	1	20	26
[Mn(Cp*)$_2$][Pt(tds)$_2$]	I	$P\bar{1}$	8.618	10.560	11.239	109.49	102.78	101.30	899	1	20	28
[Cr(Cp*)$_2$][Pt(tds)$_2$]	I	C2/c	11.352	21.848	14.969	90.00	103.73	90.00	3607	4	20	28
α-[Fe(Cp*)$_2$][Pt(mnt)$_2$]	II	C2/m	16.802	21.095	12.942	90.00	94.52	90.00	4473	6	20	16
β-[Fe(Cp*)$_2$][Pt(mnt)$_2$]	I	$P\bar{1}$	12.106	14.152	14.394	108.94	96.37	90.51	2312	3	23	16
[Fe(Cp*)$_2$]$_2$[Cu(mnt)$_2$]	IV	$P\bar{1}$	9.713	11.407	11.958	100.90	113.20	92.66	1185	1	25	29
[Fe(Cp*)$_2$][Ni(dmit)$_2$]	III	$P\bar{1}$	11.347	14.958	10.020	97.68	94.36	109.52	1575	2	-120	17
[Mn(Cp*)$_2$][Ni(dmit)$_2$]	III	$P\bar{1}$	11.415	14.940	10.020	97.40	94.58	109.63	1582	2	(a)	30
α-[Fe(Cp*)$_2$][Pd(dmit)$_2$]	III	$P\bar{1}$	9.907	12.104	14.464	82.44	85.80	82.73	1703	2	20	31
[Fe(Cp*)$_2$][Pt(dmit)$_2$]	III	$P\bar{1}$	9.996	11.554	15.108	109.72	97.62	93.78	1616	2	20	31
[Fe(Cp*)$_2$][Ni(dmio)$_2$]MeCN	IV	C2/m	16.374	10.84	19.530	90.00	88.02	90.00	3431	4	(a)	32
[Fe(Cp*)$_2$][Pd(dmio)$_2$]	III	$P\bar{1}$	14.133	14.620	16.055	88.43	80.25	86.38	3260	4	20	31
[Fe(Cp*)$_2$][Pt(dmio)$_2$]	III	$P\bar{1}$	14.133	14.620	16.055	88.43	80.25	86.38	3260	4	20	31
[Fe(Cp*)$_2$][Ni(dsit)$_2$]	III	$P\bar{1}$	9.650	11.439	16.643	71.14	73.24	89.72	1657	2	20	31
[Fe(Cp*)$_2$][Ni(bdt)$_2$]	IV	$P\bar{1}$	9.731	19.044	35.677	105.22	94.91	97.99	6266	8	20	33
[Mn(Cp*)$_2$][Ni(bdt)$_2$]	IV	$P\bar{1}$	9.760	19.101	35.606	105.02	94.72	98.15	6293	8	20	33
[Cr(Cp*)$_2$][Ni(bdt)$_2$]	IV	$P\bar{1}$	9.782	17.885	19.163	74.84	81.58	82.91	3189	4	20	33
[Mn(Cp*)$_2$][Co(bdt)$_2$]	IV	$P\bar{1}$	9.738	19.119	35.698	105.27	94.36	98.34	6298	8	20	33
[Cr(Cp*)$_2$][Co(bdt)$_2$]	IV	$P\bar{1}$	9.772	17.896	19.198	75.12	81.45	82.09	3191	4	20	33
[Fe(Cp*)$_2$][Pt(bdt)$_2$]	IV	$P\bar{1}$	7.763	19.126	35.564	104.50	95.26	97.87	6314	8	20	33
[Cr(Cp*)$_2$][Pt(bdt)$_2$]	IV	$P\bar{1}$	9.787	19.241	35.587	103.98	94.69	98.31	6387	8	20	33
[Fe(Cp*)$_2$][Ni(bds)$_2$]MeCN	IV	$P\bar{1}$	11.720	16.282	9.606	100.66	106.03	81.75	1723	2	-120	17
[Fe(Cp*)$_2$][Ni(α-tpdt)$_2$]	I	P2$_1$/c	20.360	10.237	15.443	90.00	107.54	90.00	3069	4	20	34
[Cr(Cp*)$_2$][Ni(α-tpdt)$_2$]	I	P2$_1$/c	10.053	10.281	15.577	90.00	104.89	90.00	1556	2	20	35
[Fe(C$_5$Me$_4$SCMe$_3$)$_2$][Ni(mnt)$_2$]	I	$P\bar{1}$	9.619	9.622	11.253	79.72	78.66	76.62	984	1	22	36
[Fe(C$_5$Me$_4$SCMe$_3$)$_2$][Pt(mnt)$_2$]	I	$P\bar{1}$	9.591	9.681	11.252	78.17	78.47	77.38	984	1	22	36

(a) Not given.

rangements for mixed chain ET salts based on metallocenium donors and metal bis-dichalcogenate acceptors.

While in the case of the cyano radical based salts, most of the observed structures present a type I structural arrangement, in the case of the ET salts based on metal bis-dichalcogenate acceptors a much larger variety of arrangements was observed, as described above. The structural motifs in the [M(Cp*)$_2$][M$'$(L)$_2$] ET salts are primarily determined by factors such as the dimensions of the anionic metal bis-dichalcogenate complexes, the tendency of the acceptors to associate as dimers, the extent of the π system in the acceptor molecule, and the charge density distribution on the ligands.

In the case of the [M(edt)$_2$]$^-$ based salts, with the smaller acceptor, the size of the acceptor is similar to the size of the C$_5$Me$_5$ ligand of the donor and only type I structural motifs (DADA chains) were observed. For the intermediate size

anionic complexes, $[M(tdx)_2]^-$, $[M(mnt)_2]$ and $[Ni(\alpha\text{-}tpdt)_2]^-$, the most common structural motif obtained in ET salts based on those acceptors is also of type I. For the larger anionic complexes, $[M(bdx)_2]^-$ and $[M(dmix)_2]^-$, types III and IV chain arrangements were observed, in both cases acceptor molecules (type IV) or face-to-face pairs of acceptors (type III) alternate with side-by-side pairs of donors. The complexes $[M(mnt)_2]^-$ and $[M(dmix)_2]^-$, (M = Ni, Pd and Pt), frequently undergo dimerization in the solid state [37], and they are the only acceptors where the chain arrangements have face-to-face pairs of acceptors (structural motifs II and III). The variety of structural arrangements observed in the $[M(mnt)_2]^-$ based compounds can be related to both the large extent of the π system and the high charge density on the terminal nitrile groups [38], as well as to the tendency of these complexes to form dimers.

1.2.2   ET Salts Based on Other Metallocenium Donors

Besides the decamethylmetallocenium based salts, in the compounds based on other metallocenium derivatives, mixed linear chain arrangements were only observed in the case of the salts $[Fe(C_5Me_4SCMe_3)_2][M(mnt)_2]$, M = Ni and Pt, which present type I structural motifs.

Some ET salts based on other metallocenium derivatives and on the acceptors $[M(mnt)_2]^-$ and $[M(dmit)_2]^-$ (M = Ni and Pt) have also been reported. In the case of these compounds, the crystal structure consists of segregated stacks of donors, $\cdots D^+D^+D^+D^+\cdots$, and acceptors, $\cdots A^-A^-A^-A^-\cdots$, which is a common situation in molecular materials, in particular in the case of molecular conductors. In spite of the fact that for most salts the dominant magnetic interactions between the metal bis-dichalcogenate units are antiferromagnetic, there are cases where the interactions are known to be ferromagnetic, as in the case of the compounds n-Bu$_4$N[Ni(α-tpdt)$_2$] [34] and NH$_4$[Ni(mnt)$_2$](H$_2$O, which was the first metal bis-dichalcogenate based material to present ferromagnetic ordering, with T_C = 4.5 K [7]. The unit cell parameters of the ferrocenium derivative salts with crystal structures based on segregated acceptor stacks are shown in Table 1.2.

Table 1.2. Unit cell parameters for the segregated stack salts.

Compound	Space Group	a, Å	b, Å	c, Å	α, °	β, °	γ, °	Vol., Å^3	Z	T, °C	Ref.
[Fe(Cp)$_2$]$_2$[Ni(mnt)$_2$]$_2$[Fe(Cp)$_2$]	$P\bar{1}$	12.030	13.652	15.462	87.91	77.62	72.56	2365	2	(a)	39
[Fe(C$_5$Me$_4$SMe)$_2$][Ni(mnt)$_2$]	$P\bar{1}$	8.649	14.080	15.358	65.27	77.77	80.78	1654	2	22	36
[Fe(C$_5$H$_4$R)$_2$][Ni(mnt)$_2$] (b)	P2$_1$/n	7.572	28.647	16.374	90.00	93.10	90.00	3547	4	22	40
[Fe(Cp)(C$_5$H$_4$CH$_2$NMe$_3$)][Ni(mnt)$_2$]	P2$_1$/n	12.116	30.094	7.139	90.00	103.97	90.00	2531	4	20	41
[Fe(Cp)(C$_5$H$_4$CH$_2$NMe$_3$)][Pt(mnt)$_2$]	P2$_1$/n	12.119	30.112	7.244	90.00	103.97	90.00	2565	4	20	41
[Co(Cp)$_2$][Ni(dmit)$_2$]	$P\bar{1}$	19.347	25.289	9.698	100.60	96.02	76.01	4517	8	20	42
[Co(Cp)$_2$][Ni(dmit)$_2$]$_3$2MeCN	$P\bar{1}$	8.913	21.370	7.413	99.19	91.06	101.40	1363	1	(a)	43

(a) Not given. (b) $[Fe(C_5R)_2]^+$ = 1,1'-bis[2-(4-(methylthio)-(E)-ethenyl]ferrocenium.

1.3 Solid-state Structures and Magnetic Behavior

After listing the general characteristics of the crystal structures of ET salts based on metallocenium donors and metal bis-dichalcogenate acceptors, we will discuss them based on the systematization proposed in Section 1.2 and correlate the supramolecular crystal motifs with the magnetic properties.

1.3.1 Type I Mixed Chain Salts

The magnetic behavior of the salts based on type I chains shows a considerable similarity, namely, in most cases, the dominant magnetic interactions are FM and several of these salts exhibit metamagnetic behavior. Table 1.3 summarizes the key magnetic properties of type I compounds.

1.3.1.1 $[M(Cp^*)_2][Ni(edt)_2]$

The compounds $[M(Cp^*)_2][Ni(edt)_2]$, with M = Fe and Cr, are isostructural and the crystal structure [23] consists of a parallel arrangement of 1D alternated type I chains, $\cdots A^- D^+ A^- D^+ A^- D^+ \cdots$. In Figure 1.3(a) a view along the chain direction ([101]) is presented for $[Fe(Cp^*)_2][Ni(edt)_2]$. The chains are regular and the Ni atoms sit above the Cp fragments from the donors, intrachain DA contacts, d (d = interatomic separation), shorter than the sum of the van der Waals radii (d_W), $Q_W = d/d_W < 1$, were observed. These contacts involve a Ni atom from the acceptor and one of the C atoms from the C_5 ring, with a Ni–C distance of 3.678 Å ($Q_W = 0.99$). For this compound the shortest interchain interionic separation was found in the in-registry pair II–IV, with AA C–C contacts of 3.507 Å ($Q_W = 1.11$), as shown in Figure 1.3(b). The out-of-registry pairs I–II, II–III and I–IV present a similar interchain arrangement, with DA C–S contacts (C from Me from the donor and an S from the acceptor) of 3.812 Å ($Q_W = 1.11$), the II–III pairwise arrangement is shown in Figure 1.3(c).

At high temperatures, in the case of the $[M(Cp^*)_2][Ni(edt)_2]$ compounds, AFM interactions apparently dominate the magnetic behavior of the compounds, as seen by the negative θ value obtained from the Curie–Weiss fits, −5 and −6.7 for M = Fe and Cr respectively. A considerable field dependence of the obtained θ value for polycrystalline samples (free powder) was observed in the case of $[Fe(Cp^*)_2][Ni(edt)_2]$, suggesting the existence of a strong anisotropy in the magnetic coupling for this compound [23]. This was confirmed by the metamagnetic behavior observed at low temperatures, with $T_N = 4.2$ K and $H_C = 14$ kG at 2 K.

A typical metamagnetic behavior was observed in single crystal magnetization measurements at 2 K [23], shown in Figure 1.4. With the applied magnetic field parallel to the chains a field induced transition from an AFM state to a high field FM

**Table 1.3.** Magnetic characterization of type I ET salts.

Compound	$S_D; S_A$	θ, K	Comments	Ref.
[Fe(Cp*)$_2$][Ni(edt)$_2$]	1/2; 1/2	-5	MM (a); $T_N = 4.2$ K; $H_C = 14$ kG (2 K)	23
[Cr(Cp*)$_2$][Ni(edt)$_2$]	3/2; 1/2	-6.7	(b)	23
[Fe(Cp*)$_2$][Ni(tdt)$_2$]	1/2; 1/2	15	(b)	16
[Mn(Cp*)$_2$][Ni(tdt)$_2$]	1; 1/2	2.6	MM (a); $T_N = 2.4$ K	24
[Mn(Cp*)$_2$][Pd(tdt)$_2$]	1; 1/2	3.7	MM (a); $T_N = 2.8$ K; $H_C = 0.8$ kG (1.85 K)	24
[Fe(Cp*)$_2$][Pt(tdt)$_2$]	1/2; 1/2	27	(b)	10
[Mn(Cp*)$_2$][Pt(tdt)$_2$]	1; 1/2	1.9	MM (a) $T_N = 2.3$ K;	24
[Fe(Cp*)$_2$][Ni(tds)$_2$]	1/2; 1/2	8.9	(b)	26, 44
[Mn(Cp*)$_2$][Ni(tds)$_2$]	1; 1/2	12.8	MM (a); $T_N = 2.1$ K; $H_C = 0.28$ kG (1.6 K)	28, 44
[Cr(Cp*)$_2$][Ni(tds)$_2$]	3/2; 1/2	4.0	(b)	28
[Fe(Cp*)$_2$][Pt(tds)$_2$]	1/2; 1/2	9.3	MM (a); $T_N = 3.3$ K; $H_C = 3.95$ kG (1.7 K)	26
[Mn(Cp*)$_2$][Pt(tds)$_2$]	1; 1/2	16.6	MM (a); $T_N = 5.7$ K; $H_C = 4.05$ kG (1.7 K)	28
[Cr(Cp*)$_2$][Pt(tds)$_2$]	3/2; 1/2	9.8	MM (c); $T_N = 5.2$ K; $H_{C1} = 5$ kG, $H_{C2} = 16$ kG, (1.7 K)	28
[Fe(Cp*)$_2$][Ni(α-tpdt)$_2$]	1/2; 1/2	-5.1 (d)	$T_m \approx 130$ K (e); MM (a); $T_N = 2.6$ K; $H_C = 0.6$ kG (1.6 K)	34
[Mn(Cp*)$_2$][Ni(α-tpdt)$_2$] (f)	1; 1/2	7.3	FM (g); $T_C = 2.2$ K	35
[Cr(Cp*)$_2$][Ni(α-tpdt)$_2$]	3/2; 1/2	6.1	(b)	35
[Fe(C$_5$Me$_4$SCMe$_3$)$_2$][Ni(mnt)$_2$]	1/2; 1/2	3	(b)	36
[Fe(C$_5$Me$_4$SCMe$_3$)$_2$][Pt(mnt)$_2$]	1/2; 1/2	3	(b)	36
β-[Fe(Cp*)$_2$][Pt(mnt)$_2$]	1/2; 1/2	9.8	(b)	16

(a) Metamagnetic transition. (b) No magnetic ordering observed down to 1.8 K. (c) Two field induced transitions were observed at low temperatures. (d) Non-Curie-Weiss behavior the given θ value relates to the high temperature region ($T > T_m$). (e) Minimum in χT vs. T. (f) Crystal structure not yet determined. (g) Ferromagnetic transition.

state occurs at a critical field of 14 kG. While for measurements with the applied field perpendicular to the chains, no transition was observed and a linear field dependence was observed for the magnetization, as expected for an AFM.

The magnetic behavior of [Fe(Cp*)$_2$][Ni(edt)$_2$] is consistent with the coexistence of FM intrachain interactions, due to DA intrachain short contacts, with AFM interchain interactions, resulting from the AD and AA interchain contacts. The nature of the intra and interchain magnetic interaction is in good agreement with the predictions of the McConnell I mechanism [26]. In this case the interchain interactions must be particularly large as they seem to be the dominant interactions
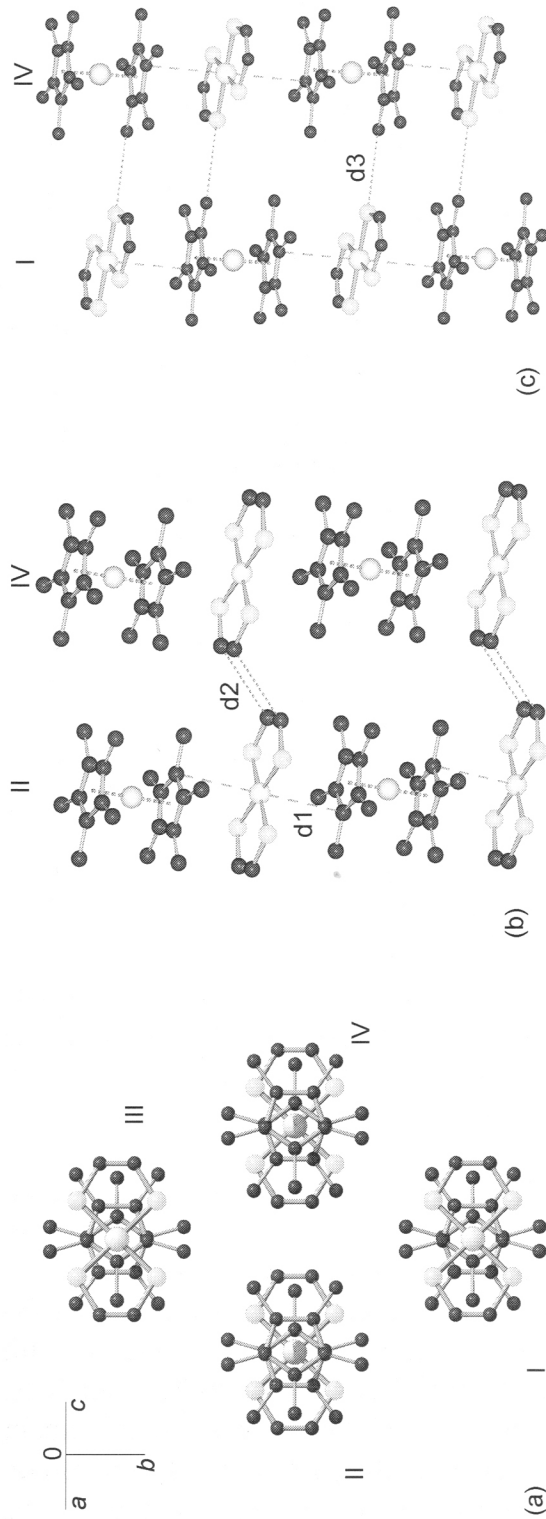
Fig. 1.3. (a) Perspective view of the crystal structure of [Fe(Cp*)$_2$]$_2$][Ni(edt)$_2$] along the chain direction. (b) Interchain arrangement of the pair II–I V, d1 corresponds to the DA closest intrachain contact (3.678 Å, Q_W = 0.99) and d2 to the closest interchain contact (3.507 Å, Q_W = 1.11). (c) Interchain arrangement of the pair II–III, d3 is the closest interchain contact (3.812 Å, Q_W = 1.11). Hydrogen atoms were omitted for clarity.
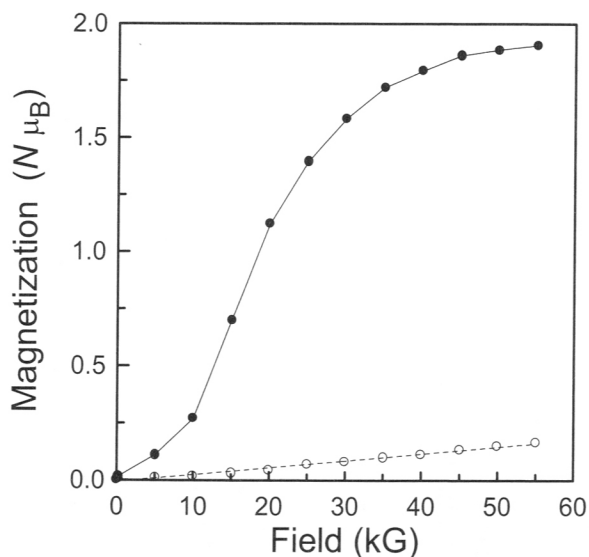
Fig. 1.4. Magnetization field dependence at 2 K, for a single crystal of [Fe(Cp*)$_2$][Ni(edt)$_2$], the closed symbols refer to measurements with applied field parallel to the DADA chains and the open symbols to the measurements with the applied field perpendicular to the chains.

at high temperatures, and they also lead to a quite high value for the critical field in the metamagnetic transition.

1.3.1.2   [M(Cp*)$_2$][M′(tdx)$_2$]

The [Fe(Cp*)$_2$][Ni(tdt)$_2$] and [Mn(Cp*)$_2$][M′(tdt)$_2$] with M′ = Ni, Pd and Pt are isostructural, and, as in the case of the [M(Cp*)$_2$][Ni(edt)$_2$] salts, a crystal structure based on an arrangement of parallel alternating DA linear chains [16] is observed, but with differences in the intra and interchain arrangements. A view normal to the chains of [Fe(Cp*)$_2$][Ni(tdt)$_2$] is shown in Figure 1.5(a). In these compounds the chains have a zigzag arrangement and the Cp sits above one of the NiS$_2$C$_2$ fragments of the acceptor, as shown for [Fe(Cp*)$_2$][Ni(tdt)$_2$] in Figure 1.5(b). In this compound, no intrachain DA short contacts were found and the closest interatomic separation between the acceptor and the Cp ring corresponds to Ni–C contacts of 4.120 Å (Q_W = 1.11). In this salt the most relevant interchain contacts concern the out-of registry pairs I–II and I–IV, these arrangements are similar and the first one is shown in Figure 1.5(b). These pairs show interchain DA C–S contacts, involving C atoms of the Me groups of the donors and S atoms of the acceptors, with a separation of 3.728 Å (Q_W = 1.08).

The magnetic behavior of the compounds [Fe(Cp*)$_2$][Ni(tdt)$_2$] and [Mn(Cp*)$_2$][M′(tdt)$_2$], with M′ = Ni, Pd and Pt, is dominated by the intrachain DA FM interactions, as seen by the positive θ values obtained from the Curie-Weiss fits (Table 1.3). At low temperatures the [Mn(Cp*)$_2$][M′(tdt)$_2$] salts exhibit metamagnetic transitions, with T_N = 2.4, 2.8 and 2.3 K for M′ = Ni, Pd and Pt respectively, H_C = 600 G for M′ = Pd [24]. This behavior is attributed to the coexistence of FM intrachain interactions with interchain AFM interactions.
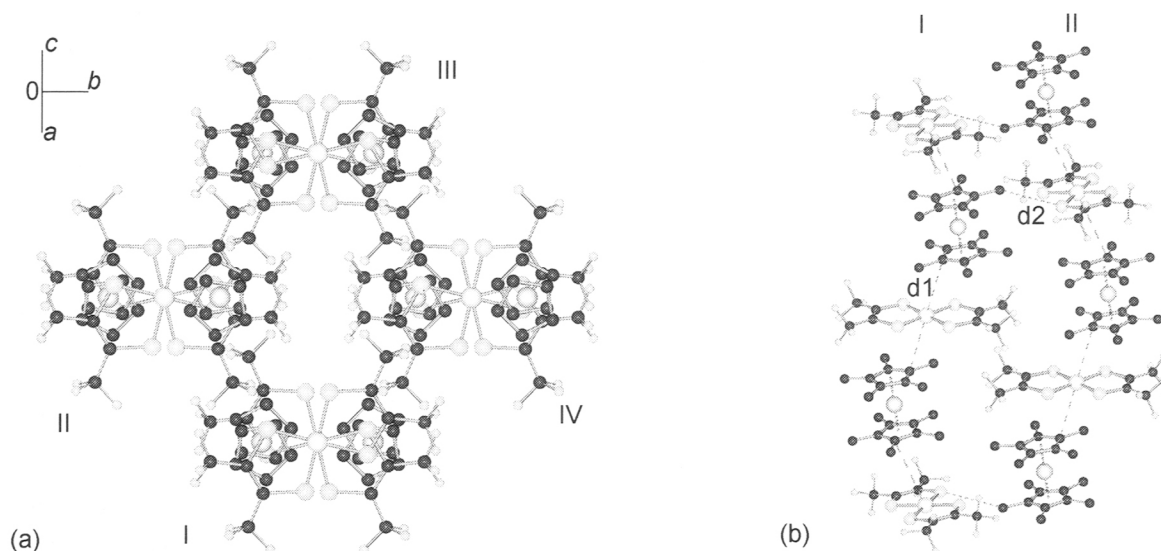
Fig. 1.5. (a) View of the crystal structure of $[Fe(Cp^*)_2][Ni(tdt)_2]$ along the chain direction (Me groups were omitted for clarity). (b) Interchain arrangement of the pair I–II, d1 corresponds to the DA closest intrachain contact (4.120 Å, $Q_W = 1.11$) and d2 to the closest interchain contact (3.728 Å, $Q_W = 1.08$). Hydrogen atoms were omitted for clarity.

The compounds $[Fe(Cp^*)_2][Pt(tdt)_2]$, $[M(Cp^*)_2][Ni(tds)_2]$, with M = Fe, Mn and Cr, [25–28] and $[M(Cp^*)_2][Pt(tds)_2]$, with M = Fe and Mn, [26, 28] are isostructural and the crystal structure consists of a parallel arrangement of alternated type I chains. The intrachain arrangement is similar to that of $[Fe(Cp^*)_2][Ni(edt)_2]$, with the Cp sitting above the Ni or Pt atoms from the acceptor, but distinct interchain arrangements were observed in these compounds. A view normal to the chains is shown in Figure 1.6(a) for $[Fe(Cp^*)_2][Pt(tds)_2]$. Short intrachain DA contacts were observed in most of these salts, involving M (Ni or Pt) and carbons from the Cp rings from the donors, for the Pt–C contact in $[Fe(Cp^*)_2][Pt(tds)_2]$ the interatomic separation is 3.826 Å ($Q_W = 0.98$). For this series of compounds the shortest interchain interionic separation was found in the in-registry pair I–II, shown in Figure 1.6(b), and it corresponds to an AA Se–Se contact, with a distance of 4.348 Å ($Q_W = 1.09$). In the other interchain arrangements the interchain contacts are considerably larger and the closest separations occur for the I–IV pair (Figure 1.6(c)) involving two C atoms from the donor Me groups, with a separation of 4.263 Å ($Q_W = 1.33$) in the case of $[Fe(Cp^*)_2][Pt(tds)_2]$. However $[Cr(Cp^*)_2][Pt(tds)_2]$ is not isostructural with these compounds, the intra and interchain arrangements are similar to those described above for $[Fe(Cp^*)_2][Pt(tds)_2]$ [28].

The magnetic behavior of the compounds $[Fe(Cp^*)_2][Pt(tdt)_2]$, $[M(Cp^*)_2][Ni(tds)_2]$ and $[M(Cp^*)_2][Pt(tds)_2]$ (M = Fe, Mn and Cr) is clearly dominated by the strong intrachain DA FM coupling, as can be seen by the high positive θ values (Table 1.3). The coexistence of an intrachain AFM interaction is responsible for the metamagnetic transitions, which are observed in several of those compounds, with T_N = 2.1, 3.3, 5.7 K and H_C = 0.28, 3.95, 4.05 kG
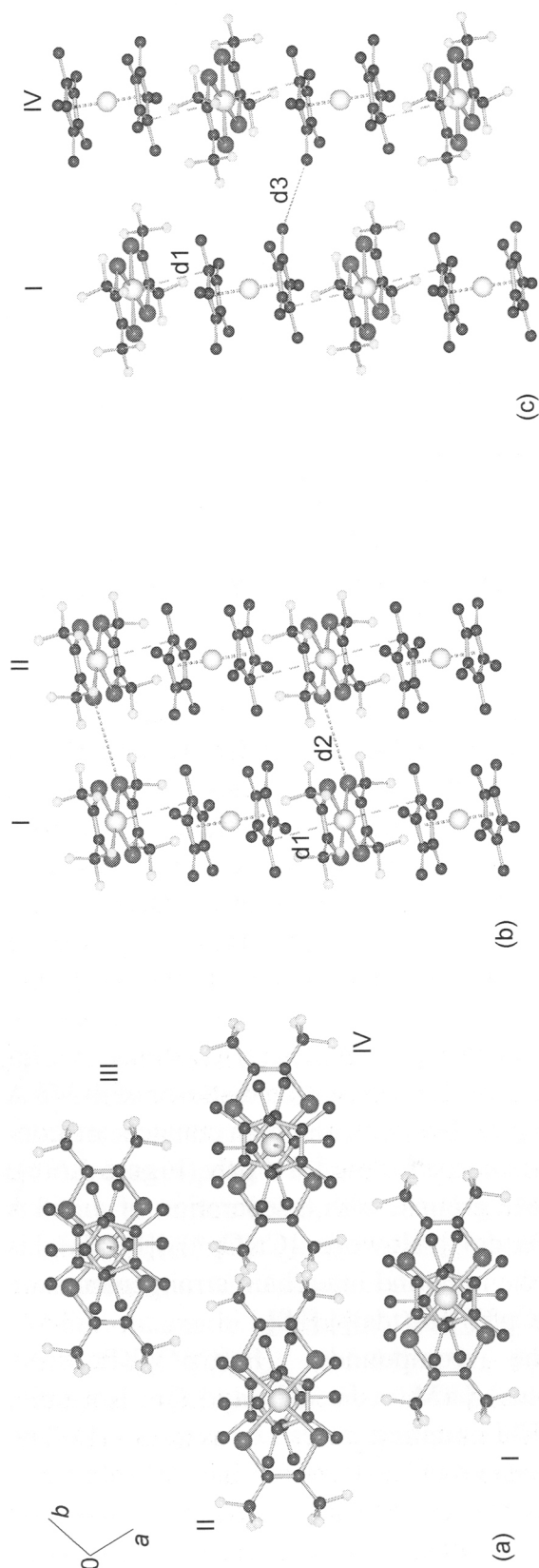
**Fig. 1.6.** (a) Perspective view of the crystal structure of [Fe(Cp*)$_2$][Pt(tds)$_2$] along the chain direction. (b) Interchain arrangement of the pair I–II, d1 corresponds to the DA closest intrachain contact (3.826 Å, $Q_W = 0.98$) and d2 to the closest interchain contact (4.348 Å, $Q_W = 1.09$). (c) Interchain arrangement of the pair I–IV, d3 is the closest interchain contact (4.263 Å, $Q_W = 1.33$). Hydrogen atoms were omitted for clarity.
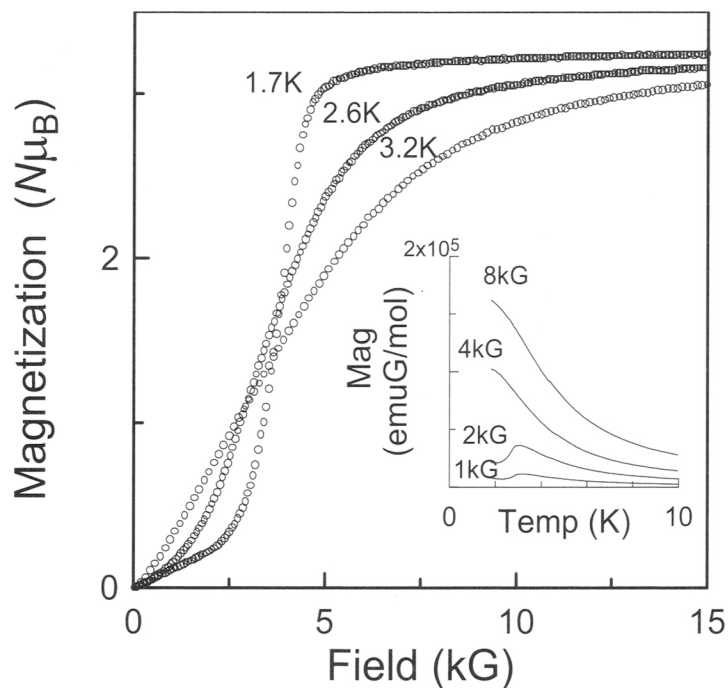
Fig. 1.7. Magnetization field dependence for [Fe(Cp*)$_2$][Pt(tds)$_2$], at 1.7, 2.6 and 3.2 K. The inset shows the magnetization temperature dependence at 1, 2, 4 and 8 kG.

for [Mn(Cp*)$_2$][Ni(tds)$_2$], [M(Cp*)$_2$][Pt(tds)$_2$] (M = Fe, Pt) respectively. The magnetization field dependence at 1.7, 2.6 and 3.2 K for [Fe(Cp*)$_2$][Pt(tds)$_2$] is shown in Figure 1.7, a sigmoidal behavior typical of metamagnetic behavior is observed for $T < T_N = 3.3$ K [26]. For low applied magnetic fields ($H < H_C$), a maximum in the magnetization temperature dependence can be observed, corresponding to an AFM transition, which is suppressed with fields $H > H_C$, as shown in the inset of Figure 1.7. The critical field temperature dependence obtained from the isothermal (closed symbols) and isofield (open symbols) measurements is shown in Figure 1.8.

In the compounds [Fe(Cp*)$_2$][Pt(tdt)$_2$], [M(Cp*)$_2$][Ni(tds)$_2$] and [M(Cp*)$_2$][Pt(tds)$_2$] (M = Fe, Mn and Cr) the Se–Se (or S–S) contacts, are expected to give rise to strong AFM interchain interactions, as the contacts are relatively short and there is a significant spin density on those atoms. The intrachain DA contacts (along c) and the interchain AA (Se–Se or S–S) contacts (along a) are expected to give rise to quasi-2D magnetic systems (ac plane), as the other interchain contacts are expected to give rise to much weaker magnetic interactions. The situation is quite distinct from that observed in the compounds [M(Cp*)$_2$][Ni(edt)$_2$], [Fe(Cp*)$_2$][Ni(tdt)$_2$] and [Mn(Cp*)$_2$][M'(tdt)$_2$], where the interchain magnetic interactions are expected to be considerably more isotropic, and for these compounds the magnetic systems can be described as quasi-1D. The distinct dimensionality of the magnetic systems is reflected in the fast saturation observed in the isothermals, just above H_C, in the case of the salts with the quasi-2D magnetic systems, unlike the compounds presenting quasi-1D magnetic
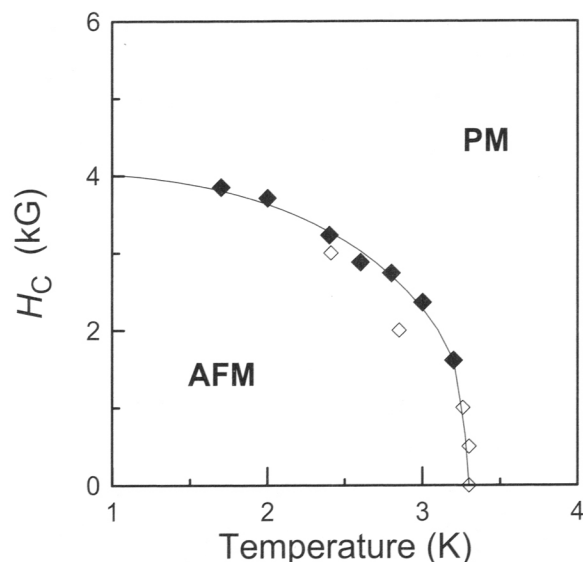
Fig. 1.8. Critical field dependence for [Fe(Cp*)$_2$][Pt(tds)$_2$], where the closed and open symbols correspond to the data obtained with isothermal and isofield measurements respectively.

systems, where saturation occurs only at very high magnetic fields, when the temperature is not much lower than T_N [26].

In the case of [Cr(Cp*)$_2$][Pt(tds)$_2$] metamagnetic behavior was also observed ($T_N = 5.2$ K), but a rather complicated phase diagram was obtained. Below T_N, two field induced transitions were observed to occur, and at 1.7 K the critical fields were 5 and 16 kG, respectively [28]. This is the first example of a metamagnetic transition on a [Cr(Cp*)$_2$] based ET salt and the low temperature phase diagram is still under study [28].

The analysis of the crystal structures, the magnetic behavior and atomic spin density calculations of several ET salts based on decamethylferrocenium and on metal-bis(dichalcogenate) acceptors with structures consisting of arrangements of parallel alternating DA linear chains, allowed a systematic study of the intra and interchain magnetic interactions [26]. In the case of these compounds a spin polarization is observed in the metallocenium donors but not in the acceptors described so far. The analysis of the intrachain contacts in the perspective of the McConnell I mechanism suggests the existence of intrachain FM coupling, through the contacts involving the metal or chalcogen atoms (positive spin density) from the acceptors and the C atoms (negative spin density) from the Cp ring of the donors, which shows good agreement with the experimental observations. A variety of interionic interchain contacts were observed in these ET salts, AA (Se–Se, S–S and C–C), DD (Me–Me) and DA (Me–S), and all these contacts were observed to lead to AFM interchain coupling. A strict application of the McConnell I model was not possible in the case of the interchain contacts, as the shortest contacts would involve mediation through H or F atoms, which are expected to present a very small spin density [26]. However the results regarding the nature of the interchain magnetic coupling would be compatible with that model if the contacts involving H or F atoms were neglected, as all the atoms involved in these contacts present a posi-

tive spin density. This study revealed that metamagnetism, which was observed in several compounds presenting a crystal structure consisting of a parallel arrangement of alternated 1D chains, is expected to occur in other compounds presenting a similar solid state structure, in the case of the metal bis-dichalcogenate acceptors no spin polarization effect is found.

1.3.1.3 $[Fe(C_5Me_4SCMe_3)_2][M(mnt)_2]$, M = Ni, Pt

The compounds $[Fe(C_5Me_4SCMe_3)_2][M(mnt)_2]$ (M = Ni, Pt) are the only cases of salts based on metallocenium derivatives and $[M(mnt)_2]^-$ complexes where the crystal structure is based on a 1D alternated type I structural motif [36]. As in the other salts described above, the crystal structure consists also of a parallel arrangement of the chains. For $[Fe(C_5Me_4SCMe_3)_2][Pt(mnt)_2]$ a view along the chains is shown in Figure 1.9(a). In the chains the $[Pt(mnt)_2]^-$ units are considerably tilted in relation to the chain direction, as shown in Figure 1.9(b), and short interatomic DA intrachain distances were observed, involving one C from the Cp and a S atom from the acceptor, with a C–S distance of 3.501 Å ($Q_W = 1.01$). Relatively short interchain interionic distances were observed in the out-of-registry pair I–IV (and the similar II–III) and in the in-registry pair II–IV. For the I–IV pair arrangement, shown in Figure 1.9(b), the shortest contact involves one S from the acceptor and a C atom from a Me group of the donor, with a S–C distance of 3.787 Å ($Q_W = 1.10$). While for the II–IV out-of-registry pair, shown in Figure 1.9(c), the shortest contact concerns one N atom from the acceptor and a C from one of the donors Me groups, with a N–C separation of 3.372 Å ($Q_W = 1.09$).

The magnetic behavior of $[Fe(C_5Me_4SCMe_3)_2][M(mnt)_2]$ (M = Ni, Pt) is dominated by FM interactions ($\theta = 3$ K, M = Ni and Pt), which can be attributed to the DA intrachain interactions. The intrachain interactions are expected to be AFM. As in the previous compounds exhibiting this type of structure metamagnetic behavior is also expected to occur at low temperatures.

1.3.1.4 β-$[Fe(Cp^*)_2][Pt(mnt)_2]$

The crystal structure of β-$[Fe(Cp^*)_2][Pt(mnt)_2]$ consists of parallel alternated $D^+A^-D^+A^-$ (type I) chains, which are isolated by chains of $D^+[A_2]^{2-}D^+$ units. A projection of the crystal structure along the stacking direction, [100], is shown in Figure 1.10(a). In the DADA chains the $[Pt(mnt)_2]^-$ are considerably tilted in relation to the chain direction, sitting on top of the ethylenic C=C of the mnt^{2-} ligands from the acceptors. A pair of the closest DADA chains (I–II) is shown in Figure 1.10(b) and they are considerably separated (16.576 Å). Short interatomic DA intrachain distances were observed, involving one C from the Cp and a S atom from the acceptor, with a C–S distance of 3.632 Å ($Q_W = 1.05$). A pair of the closest DADA chains is shown in Figure 1.10(b). One of the $D^+[A_2]^{2-}D^+$ chains
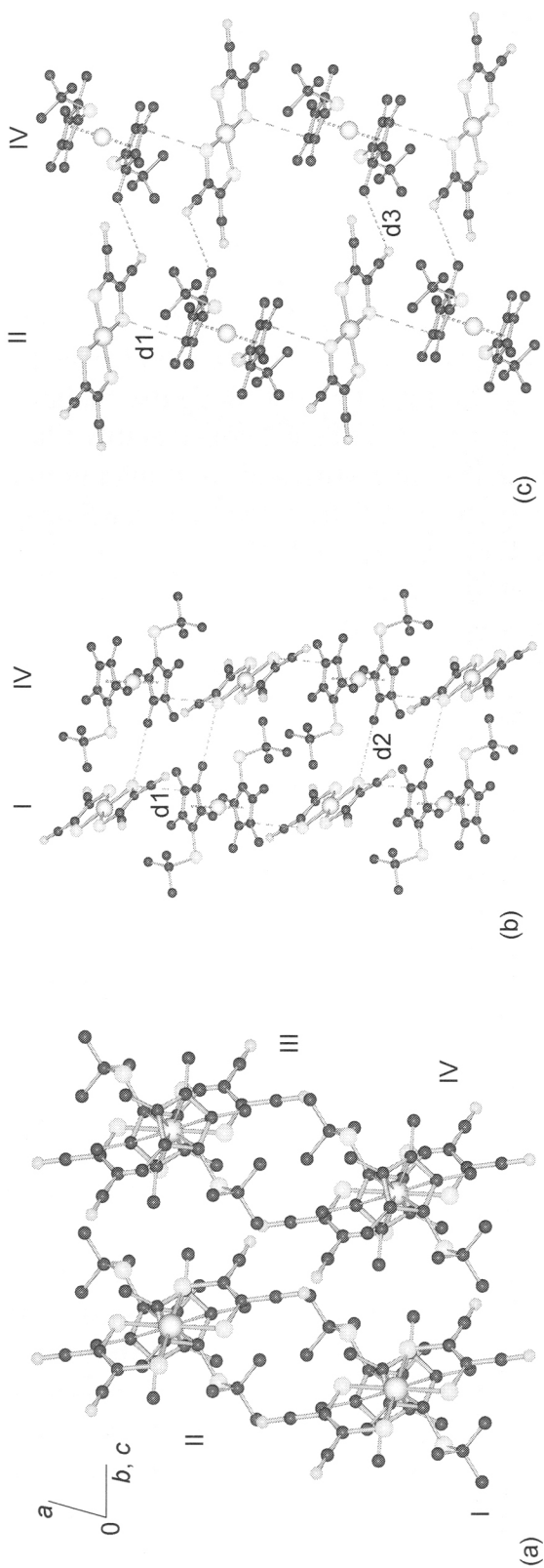
Fig. 1.9. (a) View of the structure along the chains for [Fe(C$_5$Me$_4$SCMe$_3$)$_2$][Pt(mnt)$_2$]. (b) Interchain arrangement of the pair I–IV, d1 corresponds to the DA closest intrachain contact (3.501 Å, $Q_W = 1.01$) and d2 to the closest interchain contact (3.787 Å, $Q_W = 1.10$). (c) Interchain arrangement of the pair II–IV, d3 is the closest interchain contact (3.372 Å, $Q_W = 1.09$). Hydrogen atoms were omitted for clarity.
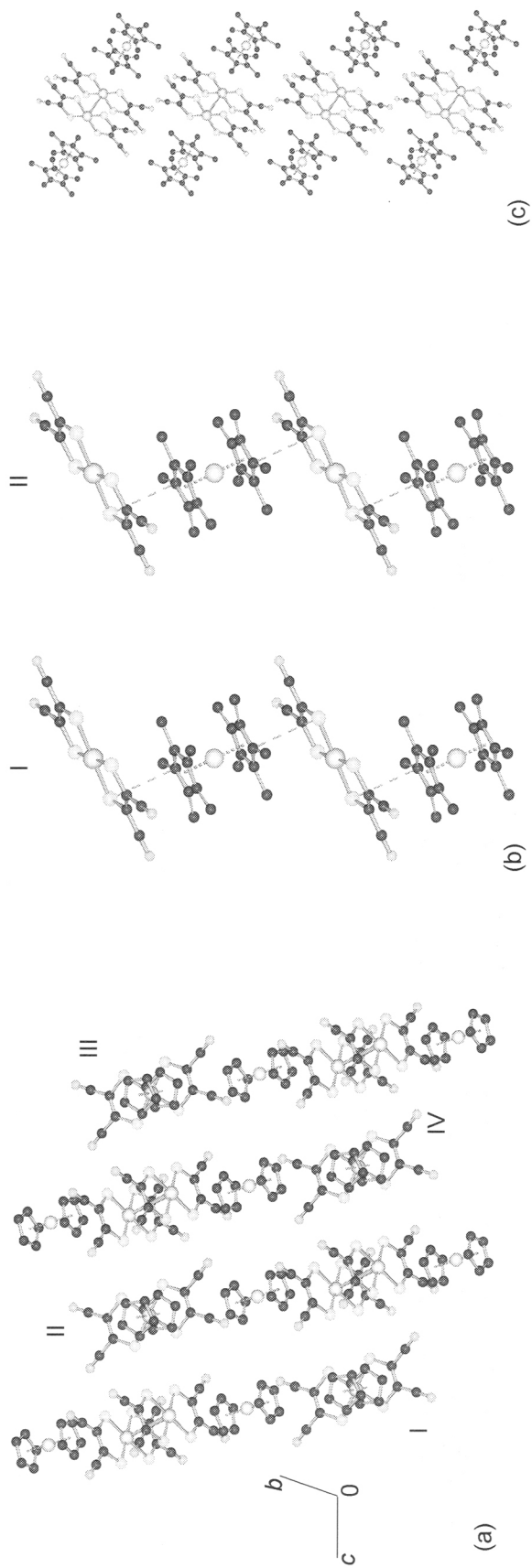
Fig. 1.10. (a) Perspective view of the structure along the DADA chain direction. (b) Interchain arrangement of the pair I–II, d1 corresponds to the DA closest intrachain contact (3.632 Å, $Q_W = 1.01$). (c) View of a $D[A_2]D$ chain. Hydrogen atoms were omitted for clarity.

is shown in Figure 1.10(c), in the DAAD units the acceptors are strongly dimerized with a Pt-Pt distance of 3.574 Å ($Q_W = 0.78$).

The magnetic susceptibility of β-[Fe(Cp*)$_2$][Pt(mnt)$_2$] follows Curie–Weiss behavior with $\theta = 9.8$ K. The dominant ferromagnetic interactions are assigned to the magnetic intrachain DA interactions from the type I chains, as the contribution from the $D^+[A_2]^{2-}D^+$ unit chains is expected to be only from the donors due to the strong dimerization of the acceptors, $S = 0$ for $[A_2]^{2-}$, and no intrachain close contacts were observed to exist.

1.3.1.5   [M(Cp*)$_2$][Ni(α-tpdt)$_2$]

The crystal structure of [Fe(Cp*)$_2$][Ni(α-tpdt)$_2$], in spite of presenting the type I structural chain motif, is considerably different from the structures presented so far [34]. The crystal structure consists of alternate layers of donors, [Fe(Cp*)$_2$]$^+$, and acceptors, [Ni(α-tpdt)$_2$]$^-$, parallel to the *ab* plane (*ab* layers). A projection of the crystal structure along a is shown in Figure 1.11(a) for [Fe(Cp*)$_2$][Ni(α-tpdt)$_2$]. In the acceptor layers, relatively short interionic AA distances were found, involving S atoms from the central NiS$_4$ fragment and a C atom from the thiophenic fragment of the ligand, as shown Figure 1.11(b). The S$\cdots$C separations are 3.723 and 3.751 Å, exceeding the sum of the van der Waals radii (3.450 Å) by 8 and 9% respectively. Short interlayer interionic DA distances were found, involving C atoms from the Cp rings and the S atom from the thiophenic fragment from the acceptors, with S$\cdots$C distances of 3.530 and 3.610 Å, exceeding the sum of the van der Waals radii by 2 and 5% respectively. These contacts give rise to a set of layers (*bc* layers) composed of parallel alternated DADA chains, as shown in Figure 1.11(c). The chains in adjacent layers are almost perpendicular to each other, running along directions alternating from $2b + c$ to $2b - c$. Two chains from adjacent layers are shown in Figure 1.11(d) along with two anionic ab layers.

The chains in the bc layers present an out-of registry arrangement. Short interionic DA interchain distances were observed, involving a S from the MS$_2$C$_2$ fragment from the acceptor and a C from the Me groups in the donor, with S-C separations exceeding the sum of the van der Waals radii by less than 8%, as shown in Figure 1.11(c). The contacts between the chain in adjacent layers correspond to the (S–C) AA contacts previously mentioned in the case of the acceptor ab layers.

The compounds [M(Cp*)$_2$][Ni(α-tpdt)$_2$], M = Fe and Cr, although not isostructural, present a similar solid state structure. In the case of [Cr(Cp*)$_2$][Ni(α-tpdt)$_2$] the crystal structure is more symetric than the analogue with M = Fe. The contacts are of the same order and the most significant difference between the two structures is the arrangement of the molecules in the acceptor ab layers, unlike the case of [Fe(Cp*)$_2$][Ni(α-tpdt)$_2$], where there was only one type of relevant AA contact, because of a short S–C distance, for [Cr(Cp*)$_2$][Ni(α-tpdt)$_2$], the S atom (from the central NiS$_4$ fragment) is close to two distinct C atoms from the thiophenic
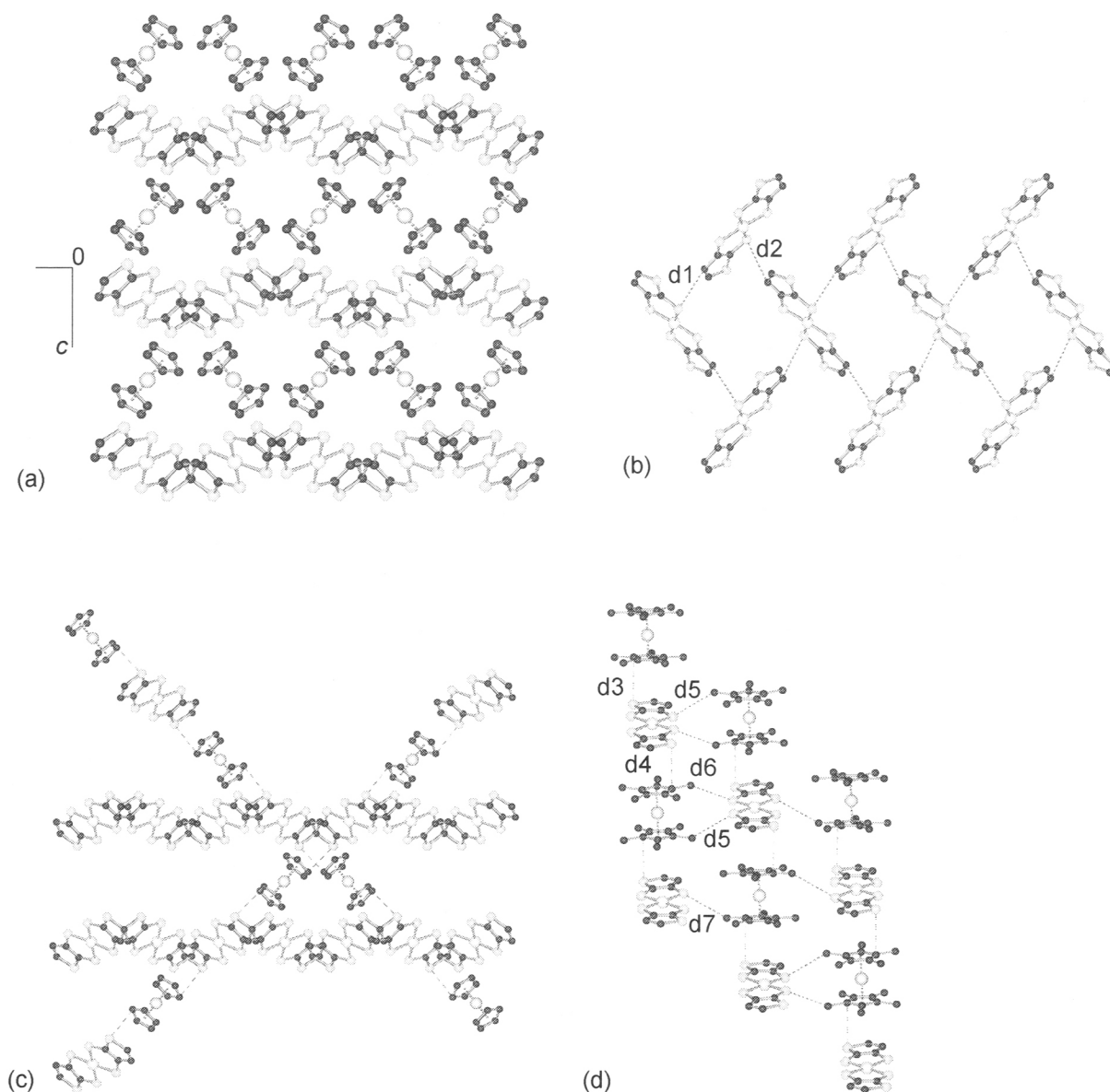
Fig. 1.11. Projection of the structure along a for [Fe(Cp*)$_2$][Ni(α-tpdt)$_2$] (Me groups were omitted for clarity). (b) View of an acceptor layer, showing the closest AA separations (S–C) d1 and d2 (3.775 and 3.721 Å, Q_W = 1.09 and 1.08). (c) Partial view of the crystal structure illustrating two consecutive anionic layers and two orthogonal DADA chains. (d) View of the structure showing parallel DADA chains, the shortest interionic separations are shown, d3 and d4 correspond to the intrachain contacts (3.519 and 3.622 Å, Q_W = 1.02 and 1.05) and d5-d7 are interchain DA (S–C) separations (3.671, 3.694, 3.722 Å, Q_W = 1.06, 1.06 and 1.08). Hydrogen atoms were omitted for clarity.

fragment, with separations of the same order, 3.768 and 3.756 Å (Q_W = 1.09 and 1.08). However the closest contact involves the same C in both compounds.

In the case of the compound [Fe(Cp*)$_2$][Ni(α-tpdt)$_2$] [34] a minimum is observed in the temperature dependence of the χT product. at 130 K, which is consistent either with ferrimagnetic behavior or with a change in the type of the dominant magnetic interactions. A Curie–Weiss fit to the experimental data in the high

temperature regime gave a θ value of -5.1 K. At low temperatures metamagnetic behavior was observed in the case of [Fe(Cp*)$_2$][Ni(α-tpdt)$_2$], with $T_N = 2.6$ K and $H_C = 600$ G, at 1.7 K. The temperature dependence of H_C is shown in Figure 1.12. In the case of [M(Cp*)$_2$][Ni(α-tpdt)$_2$], with M = Mn and Cr [35], at high temperatures, the magnetic susceptibility follows a Curie–Weiss behavior, with θ values of 7.3 and 6.1 K, showing dominant ferromagnetic interactions for these compounds. A FM transition that was observed to occur in case of [Mn(Cp*)$_2$][Ni(α-tpdt)$_2$], at 2.2 K, as denoted by a maximum observed in the real and imaginary contributions of the ac susceptibility. No hysteresis was observed in the isothermals below $T_C = 2.2$ K, for low applied magnetic fields, the magnetization isothermals showed a drastic increase and a very slow and nearly linear increase is observed above 5 kG ($M = 2.5 \, N \, \mu_B$), reaching a value of 3.0 $N \, \mu_B$ at 120 kG, which is consistent with the spin only ($g_A = g_D = 2.0$) value for the saturation magnetization, $M_{sat} = g_A S_A + g_D S_D = 3.0 \, N \, \mu_B$. The poor quality of the crystals of this compound has so far prevented crystal structure determination, however a crystal structure similar to that observed for the Fe and Cr analogues, is expected for this compound.

Unlike the previously mentioned acceptors, calculations predict a spin polarization effect in the case of [Ni(α-tpdt)$_2$]$^-$, and small negative spin densities are expected in the S atom and in one of the carbons from the thiophenic ring [35]. As a consequence a competition between FM and AFM (DA or AA) interactions is expected. From the room temperature crystal structure analysis the stronger interionic contact is expected to be AFM as it corresponds to the intrachain DA contact involving two atoms with negative spin densities, a S from the thiophenic ring of the acceptor and a C from the C$_5$ ring of the donor. The shorter AA contacts from the anionic layers are expected to give rise to FM interactions, as the spin densities of the atoms do not have the same sign. The high temperature magnetic behavior of the [M(Cp*)$_2$][Ni(α-tpdt)$_2$] salts indicates AFM dominant interactions, which is consistent with the McConnell I model predictions for the DA interactions. However the change in the nature of the magnetic interactions in the case of [Fe(Cp*)$_2$][Ni(α-tpdt)$_2$], remains an open question. This change can be attributed to small variations in the interionic contacts on cooling. In both intrachain DA and interlayer AA arrangements, besides the shorter contacts referred to before, there are also slightly longer interionic separations, which could lead to different types of interactions for both the DA and AA contacts. As observed in the [Fe(Cp*)$_2$] based compound, in the case of [Cr(Cp*)$_2$][Ni(α-tpdt)$_2$], the shorter contacts involve atoms with the same spin density parity (AFM coupling) and a competition between AFM and FM interactions is expected. The experimental results indicate that in this case the FM interactions dominate the magnetic behavior of this compound. The distinct magnetic behavior found in [M(Cp*)$_2$][Ni(α-tpdt)$_2$], with M = Fe, Mn and Cr, can be related to the competition between the FM and AFM interactions and the small differences in the DA overlap observed in the DADA chains. The poor quality of the crystals of [Mn(Cp*)$_2$][Ni(α-tpdt)$_2$] has so far
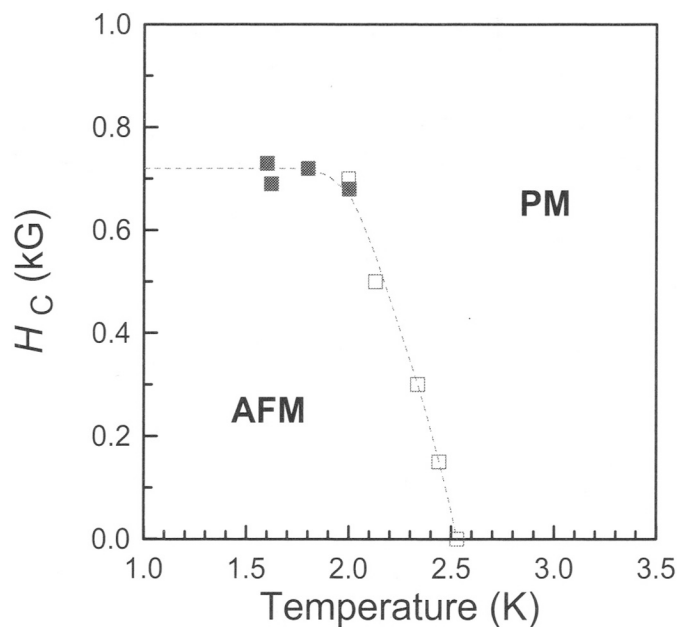
Fig. 1.12. Critical field dependence for $[Fe(Cp^*)_2][Ni(\alpha\text{-tpdt})_2]$, where the closed and open symbols correspond to the data obtained with isothermal and isofield measurements respectively.

prevented crystal structure determination, however a crystal structure similar to that observed for the Cr analogue is expected for this compound, considering the magnetic behavior observed in these compounds.

1.3.2   Type II Mixed Chain $[M(Cp^*)_2][M'(L)_2]$ Salts

This type of chain arrangement was observed only in the case of α-$[Fe(Cp^*)_2][Pt(mnt)_2]$. In the crystal structure, layers of parallel DAADAA (type II) chains, with a net charge $(-)$ per repeat unit, $[A_2]^{2-}D^+$, alternate with layers presenting a $D^+D^+A^-$ repeating unit, with a net $(+)$ per repeat unit [16]. A view of the crystal structure along the type II chain direction, [100], is shown in Figure 1.13(a). In the type II chain layers the acceptors are strongly dimerized with a Pt–Pt distance of 3.575 Å ($Q_W = 0.78$) and the $[A_2]^{2-}D^+[A_2]^{2-}D^+$ chains present an out-of-registry arrangement, as shown in Figure 1.13(b). Apart from the AA contacts no other short contacts were observed in these layers. The DDA layer presents a unique arrangement, where the donors sit on top of the extremity of the acceptors, these DDA units form edge to edge chains, as shown in Figure 1.13(c). In these layers the closest interionic separations involve one C from the Cp and a S atom from the acceptor, with a C–S distance of 3.952 Å ($Q_W = 1.15$).

The magnetic susceptibility of α-$[Fe(Cp^*)_2][Pt(mnt)_2]$ follows Curie–Weiss behavior with $\theta = 6.6$ K [16]. The dominant ferromagnetic interactions are assigned to the magnetic DA interactions from the DDA layers, as the contribution from the $[A_2]^{2-}D^+$ chains is expected to be only from the isolated donors due to the strong dimerization of the acceptors, $S = 0$ for $[A_2]^{2-}$.
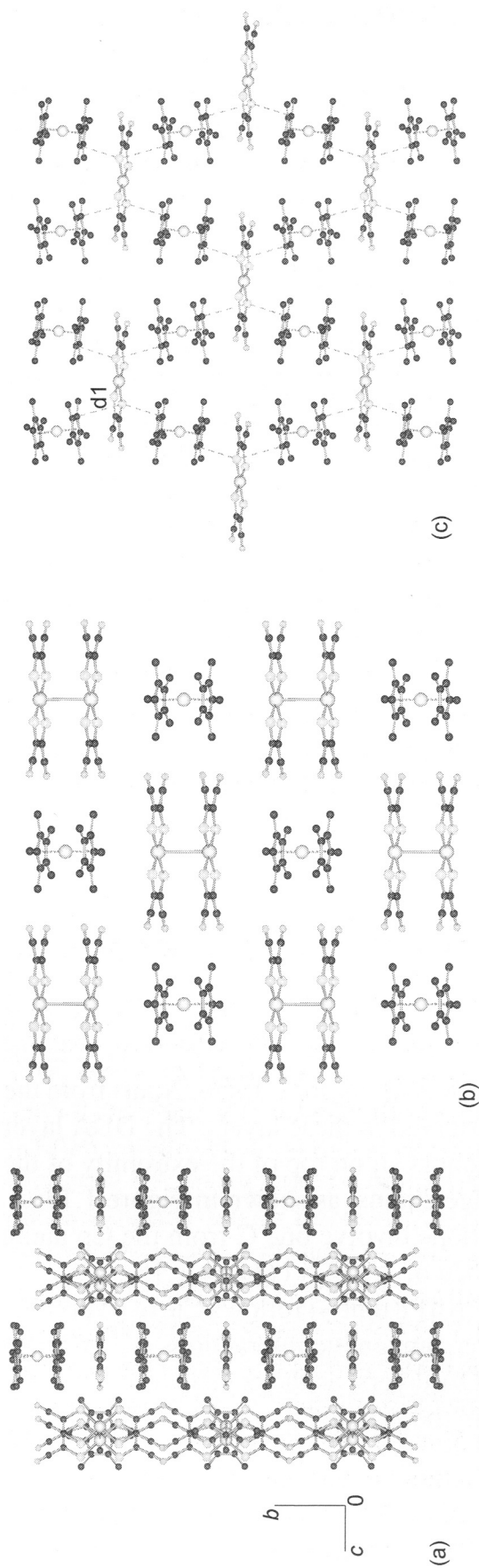
Fig. 1.13. (a) View of the structure of α-[Fe(Cp*)$_2$][Pt(mnt)$_2$] along the DAADAA (type II) chains. (b) View of a type II chain layer. (c) View of the DDA layer, d1 corresponds to the closest contact (3.952 Å, $Q_W = 1.15$). Hydrogen atoms were omitted for clarity.

1.3.3   Type III Mixed Chain [M(Cp*)$_2$][M′(L)$_2$] Salts

The acceptor-acceptor magnetic interactions play a key role in the magnetic behavior of the [M(Cp*)$_2$][M′(L)$_2$] salts based on type III chains, and in most cases the AA interactions are AFM. Table 1.4 summarizes the key magnetic properties of type III [M(Cp*)$_2$][M′(L)$_2$] compounds.

**Table 1.4.** Magnetic characterization of type III [M(Cp*)$_2$][M′(L)$_2$] salts.

Compound	S_D; S_A	θ, K	Comments	Ref.
[Fe(Cp*)$_2$][Ni(dmit)$_2$]	1/2; 1/2	−7.6 (a)	(b); $T_m = 30$ K (c)	45
[Mn(Cp*)$_2$][Ni(dmit)$_2$]	1; 1/2	2 (d)	FM (e); $T_C = 2.5$ K	46
α-[Fe(Cp*)$_2$][Pd(dmit)$_2$]	1/2; 1/2	−22.3	(b)	31
β-[Fe(Cp*)$_2$][Pd(dmit)$_2$] (f)	1/2; 1/2	2.6	(b)	45
[Fe(Cp*)$_2$][Pt(dmit)$_2$]	1/2; 1/2	−14.4	(b)	45
[Fe(Cp*)$_2$][Ni(dmio)$_2$] (f)	1/2; 1/2	−19.0	(b)	45
[Fe(Cp*)$_2$][Pd(dmio)$_2$]	1/2; 1/2	−24.7	(b)	45
[Fe(Cp*)$_2$][Pt(dmio)$_2$]	1/2; 1/2	−33.3	(b)	45
[Fe(Cp*)$_2$][Ni(dsit)$_2$]	1/2; 1/2	−18.9	(b)	31

(a) Non-Curie–Weiss behavior the given θ value relates to the high temperature region ($T > T_m$). (b) No magnetic ordering down to 1.8 K. (c) Minimum in χT vs. T. (d) Estimated value from χT vs. T plot in Ref. [46]. (e) Ferromagnetic transition. (f) Crystal structure not yet determined.

1.3.3.1   [M(Cp*)$_2$][M′(dmit)$_2$] (M = Fe; M′ = Ni, Pt and M = Mn; M′ = Ni)

The salts [Fe(Cp*)$_2$][M(dmit)$_2$], with M = Ni [17] and Pt [31], and [Mn(Cp*)$_2$][Ni(dmit)$_2$] [30] are isostructural and the crystal structure consists of 2D layers composed of parallel type III chains, $\cdots A^- A^- D^+ D^+ A^- A^- D^+ D^+ \cdots$, where face-to-face pairs of acceptors alternate with side-by-side pairs of donors. A view of the structure along the chain direction is shown in Figure 1.14(a) for [Fe(Cp*)$_2$][Ni(dmit)$_2$]. The chains are regular and the Cp fragments of the donor sit above dmit ligands of the acceptor, as shown for [Fe(Cp*)$_2$][Ni(dmit)$_2$] in Figure 1.14(b). Intrachain AA short contacts are observed in the [Ni(dmit)$_2$]$^-$ dimers, involving a Ni atom and one of the sulfur atoms from the five-membered C$_2$S$_2$C ring from the ligand, with a Ni–S distance of 3.792 Å ($Q_W = 0.96$). The intrachain DA separation is considerably larger and the shorter contacts between the acceptor and the Cp rings correspond to a S–C contact (S from the C$_2$S$_2$C fragment) with distances of 3.611 and 3.659 Å ($Q_W = 1.05$ and 1.06). Several short AA (S–S) interchain contacts were observed in this compound and the crystal structure can be better described as being based on layers of out-of-registry parallel chains, one of these layers is shown in Figure 1.14(b). The intralayer interchain contacts are
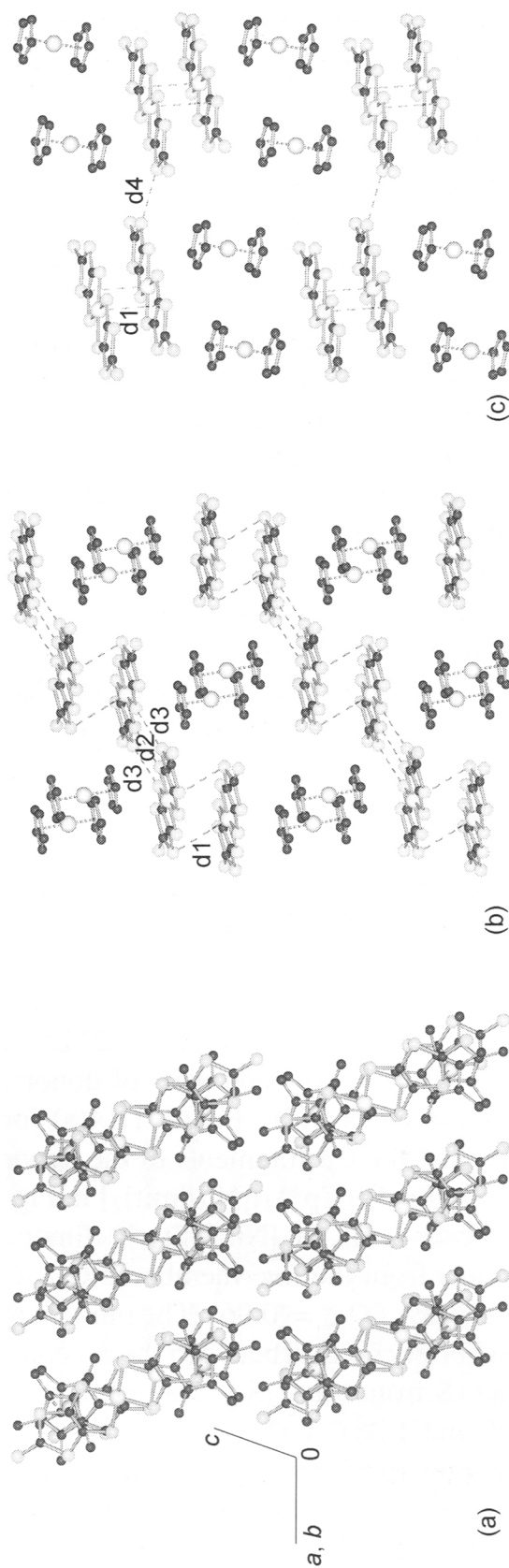
Fig. 1.14. (a) Perspective view of the crystal structure of $[Fe(Cp^*)_2][Ni(dmit)_2]$ along the stacking direction (hydrogen atoms were omitted for clarity). (b) View of one layer of the type II chains, d1 corresponds to the intradimer (AA) closest contact (3.792 Å, $Q_W = 0.96$), and d2 and d3 to short interchain contacts (3.422 and 3.547 Å, $Q_W = 0.93$ and 0.96) (Me groups were omitted for clarity). (c) View of two neighboring chains from different layers, d4 is the closest interlayer contact (3.375 Å, $Q_W = 0.91$) (Me groups were omitted).

shorter than the intrachain and two types of contacts are observed. The longer contact involves one of the S from the central MS_4 fragment and one of the S from the ligand C_2S_2C fragment, with a S–S distance of 3.547 Å ($Q_W = 0.96$), and the shorter contact involves two S atoms from the central MS_4 fragment, with a S–S distance of 3.422 Å ($Q_W = 0.93$). There are also interchain interlayer AA short contacts, involving S atoms from the C_2S_2C ligand fragments, with a S–S distance of 3.375 Å ($Q_W = 0.91$), as shown in Figure 1.14(c).

In spite of the similarities in the crystal structures of the compounds [Fe(Cp*)$_2$][M(dmit)$_2$], with M = Ni and Pt, and [Mn(Cp*)$_2$][Ni(dmit)$_2$], they present distinct magnetic behaviors. In the case of [Fe(Cp*)$_2$][M(dmit)$_2$], a minimum in the temperature dependence of χT, is observed at 30 K [45], as shown in Figure 1.15. This can be attributed to a change in the dominant magnetic interactions, due to structural changes on cooling. At high temperatures the magnetic susceptibility follows Curie-Weiss behavior, with a θ value of -7.6 K, which clearly indicates that AFM interactions are dominant. However, below $T_m = 30$ K, χT increases rapidly, indicating that FM become dominant in that region, this is further confirmed by the magnetization field dependence at low temperatures, which for low applied magnetic fields increases faster than predicted by the Brillouin function (solid line) and at high fields slowly approaches the saturation magnetization, as shown in Figure 1.16. In the case of [Mn(Cp*)$_2$][Ni(dmit)$_2$] a FM transition was reported to occur at 2.5 K [46], the field cooled (FCM), zero field cooled (ZFCM) and remnant (REM) magnetization temperature dependences are shown in Figure 1.17. This is the first and only case, to date, in this class of compounds to present FM ordering and this behavior was analyzed in the light of the McConnell I mechanism, namely for the intradimer magnetic interactions due to a spin polarization effect in the acceptor molecules. According to the McConnell I model these interactions are predicted to be FM as the atoms involved in the intradimer contacts
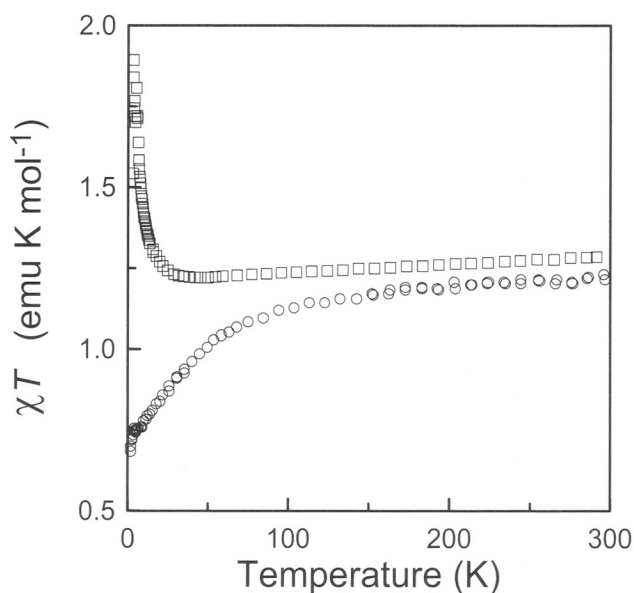
Fig. 1.15. χT temperature dependence for [Fe(Cp*)$_2$][Ni(dmit)$_2$] (squares) and [Fe(Cp*)$_2$][Pt(dmit)$_2$] (circles).
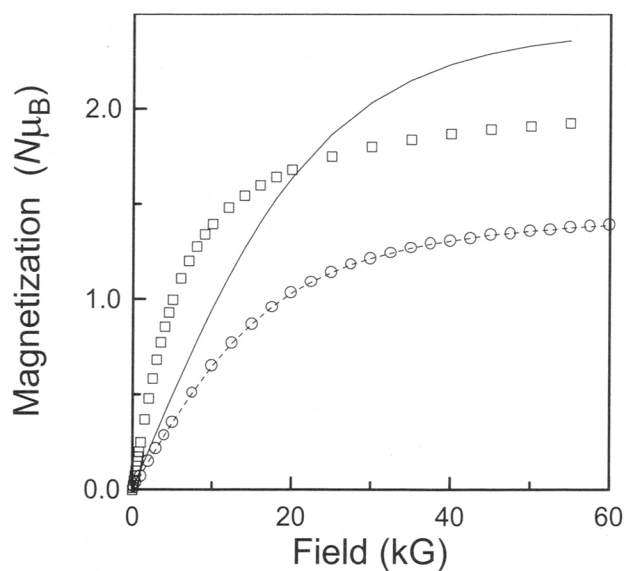
Fig. 1.16. Magnetization field dependence for [Fe(Cp*)$_2$][Ni(dmit)$_2$] (squares) and [Fe(Cp*)$_2$][Pt(dmit)$_2$] (circles) at 1.8 K. The solid line corresponds to the Brillouin function considering the donor and acceptor spins, while the dashed line corresponds only to the contribution from the donor molecules.
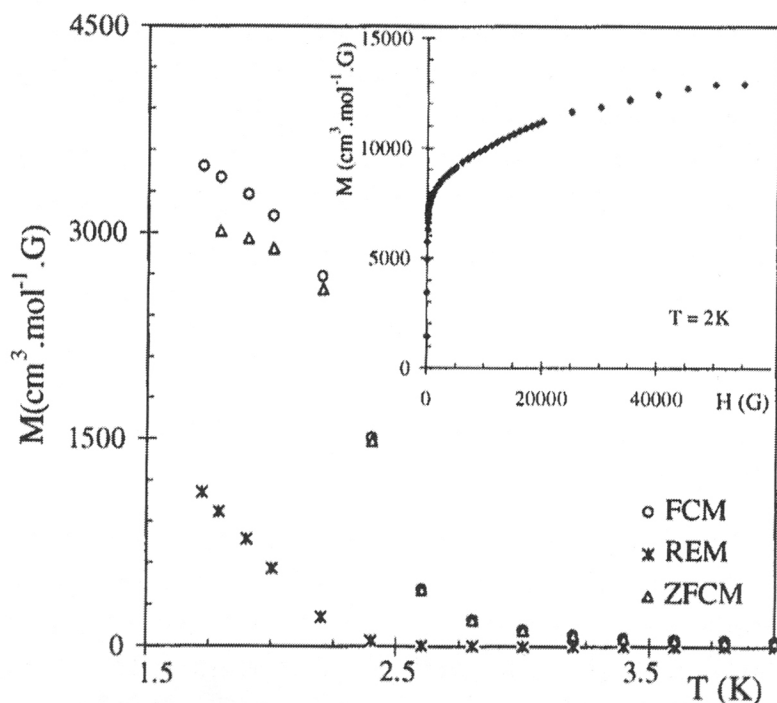
Fig. 1.17. Field-cooled (FCM), zero-field-cooled (ZFCM) and remnant (REM) magnetization temperature dependences of [Mn(Cp*)$_2$][Ni(dsit)$_2$] (reproduceded with permission from Ref. [46]).

present different signs in the atomic spin density, the Ni atom presents a positive spin density while in the S atoms from the C$_2$S$_2$C ligands fragments, the spin density is negative [47]. In the case of [Fe(Cp*)$_2$][Pt(dmit)$_2$] the magnetic behavior is dominated by AFM interactions as the magnetic susceptibility follows Curie–Weiss behavior, with a θ value of -14.4 K [45], and the χT product decreases on cooling, as shown in Figure 1.15. For this compound the magnetization isothermals (circles in Figure 1.16) at low temperature are consistent with total cancella-

tion of the magnetic contribution from the acceptors, and the magnetization field dependence follows the Brillouin function for the isolated donors, $[Fe(Cp^*)_2]^+$, (dashed line) as shown in Figure 1.16. In the case of $[Fe(Cp^*)_2][M(dmit)_2]$ (M = Ni and Pt), the S–S intra and interlayer short contacts are expected to lead to AFM interactions, as the spin density of the atoms involved in the shorter contacts have the same sign. Considering that these contacts are even shorter than the intradimer ones (FM coupling), dominant AFM interactions are expected, which is consistent with the observed negative θ values for $[Fe(Cp^*)_2][Pt(dmit)_2]$, and for $[Fe(Cp^*)_2][Ni(dmit)_2]$, at high temperatures. The change in behavior observed in the case of $[Fe(Cp^*)_2][Ni(dmit)_2]$, can originate from a weakening of the intra and interlayer AFM interactions. It is worth mentioning that, in the case of the interchain intralayer interactions, the shorter contacts (involving two S atoms from the central MS_4 fragment) are expected to be AFM, while the weaker contacts (involving a S from the central MS_4 fragment and one of the S from the C_2S_2C fragment) are predicted to give rise to FM interactions. In this case a slight change in the interionic arrangement could change the nature of the intralayer magnetic interactions. A similar situation was reported in the case of $NH_4[Ni(mnt)_2] \cdot H_2O$, which shows dominant AFM interactions at high temperatures ($T > 100$ K), for low temperatures FM interactions become dominant and ferromagnetic ordering is exhibited at 4.5 K [7]. The magnetic behavior of $[Fe(Cp^*)_2][Ni(dmit)_2]$ is still puzzling and requires further study.

1.3.3.2 $[Fe(Cp^*)_2][M(dmio)_2]$ (M = Pd and Pt), α-$[Fe(Cp^*)_2][Pd(dmit)_2]$ and $[Fe(Cp^*)_2][Ni(dsit)_2]$

The compounds $[Fe(Cp^*)_2][M(dmio)_2]$, with M = Pd and Pt, are isostructural and the crystal structure consists of a parallel arrangement of 1D type III chains. The solid state structure is similar to that observed in $[Fe(Cp^*)_2][Ni(dmit)_2]$ and presents a similar layered motif. However, for $[Fe(Cp^*)_2][M(dmio)_2]$ (M = Ni and Pt) the dimers show a different configuration, in this case no slippage is observed in the dimer and a short Pd–Pd contact was observed in the case of $[Fe(Cp^*)_2][Pd(dmio)_2]$, with a Pd–Pd distance of 3.481 Å ($Q_W = 0.76$). In this compound short intralayer AA contacts were also detected, involving a S from the central MS_4 fragment and one of the S from the C_2S_2C fragment, with a S–S distance of 3.669 Å ($Q_W = 0.99$). No interlayer short contacts were observed for $[Fe(Cp^*)_2][Pd(dmio)_2]$. The compound α-$[Fe(Cp^*)_2][Pd(dmit)_2]$ is not isostructural with $[Fe(Cp^*)_2][M(dmio)_2]$, with M = Pd and Pt, but presents a similar molecular arrangement in the crystal structure. Again, in the case of α-$[Fe(Cp^*)_2][Pd(dmit)_2]$, a strong dimerization was observed for the acceptors, presenting also short Pd–Pd contacts, with a distance of 3.485 Å ($Q_W = 0.76$). Short intralayer contacts, similar to those observed in the previous compound, were ob-

served, with a S–S distance of 3.558 Å ($Q_W = 0.96$). No interlayer short contacts were observed for α-[Fe(Cp*)$_2$][Pd(dmit)$_2$].

The magnetic susceptibility of [Fe(Cp*)$_2$][M(dmio)$_2$] (M = Pd and Pt) and α-[Fe(Cp*)$_2$][Pd(dmit)$_2$] follows Curie–Weiss behavior, with θ values of -24.7, -33.3 and -22.3 K, respectively. The magnetic behavior is clearly dominated by the AFM intradimer interactions. At low temperatures, the magnetic field dependence follows the predicted values for the isolated donors, as in the case of [Fe(Cp*)$_2$][Pt(dmit)$_2$]. Unlike the [Ni(dmit)$_2$] and [Pt(dmit)$_2$] based compounds, for [Fe(Cp*)$_2$][M(dmio)$_2$] (M = Pd and Pt) and [Fe(Cp*)$_2$][Pd(dmit)$_2$] the short intradimer contacts are expected to lead to strong AFM interactions, which is in agreement with the experimental observations.

The crystal structure of [Fe(Cp*)$_2$][Ni(dsit)$_2$] is similar to those described previously in this section. In this salt the acceptors are strongly dimerized through Ni–Se bonds, the Ni(dsit)$_2$ units are slipped (see Figure 1.18) and the metal adopts a square pyramidal conformation, with an apical Ni–Se distance of 2.555 Å, which is slightly larger than the average equatorial Ni–Se bond distance, 2.330 Å.

The magnetic susceptibility of [Fe(Cp*)$_2$][Ni(dsit)$_2$] follows Curie–Weiss behavior, with a θ value of -19.8 K. The magnetic behavior is clearly dominated by the AFM intradimer interactions. At low temperatures, the magnetic field dependence follows the predicted values for the isolated donors, as in the case of the analogous compounds presenting dominant AFM interactions, described previously.

In the case of β-[Fe(Cp*)$_2$][Pd(dmit)$_2$] dominant FM interactions ($\theta = 2.6$ K) were observed and the crystal structure in this compound is expected to be similar either to that described for [Fe(Cp*)$_2$][Ni(dmit)$_2$] or to that reported for [Fe(Cp*)$_2$][Ni(dmio)$_2$]MeCN, which will be described in the next section (Section 1.3.4.1.). For [Fe(Cp*)$_2$][Ni(dmio)$_2$] the observed large negative θ value (-19 K) suggests that this compound must present a crystal structure similar to those reported for the Pd and Pt analogues or for α-[Fe(Cp*)$_2$][Pd(dmit)$_2$].

The supramolecular arrangement in the type III chain based salts, at high temperatures, is consistent with the existence of dominant AFM interactions through AA interactions. For the compounds with dominant FM interactions at low temperatures, the magnetic behavior can be related to the distinct dimer arrangements. The dimer arrangements along with the dimer overlap are illustrated in Figure 1.18, for [Fe(Cp*)$_2$][Ni(dmit)$_2$] α-[Fe(Cp*)$_2$][Pd(dmit)$_2$] and [Fe(Cp*)$_2$][Ni(dsit)$_2$]. As stated before the contacts in the case of [Fe(Cp*)$_2$][Ni(dmit)$_2$] are expected to give rise to FM intradimer interactions, while in the case of the other two compounds AFM intradimer interactions are anticipated.
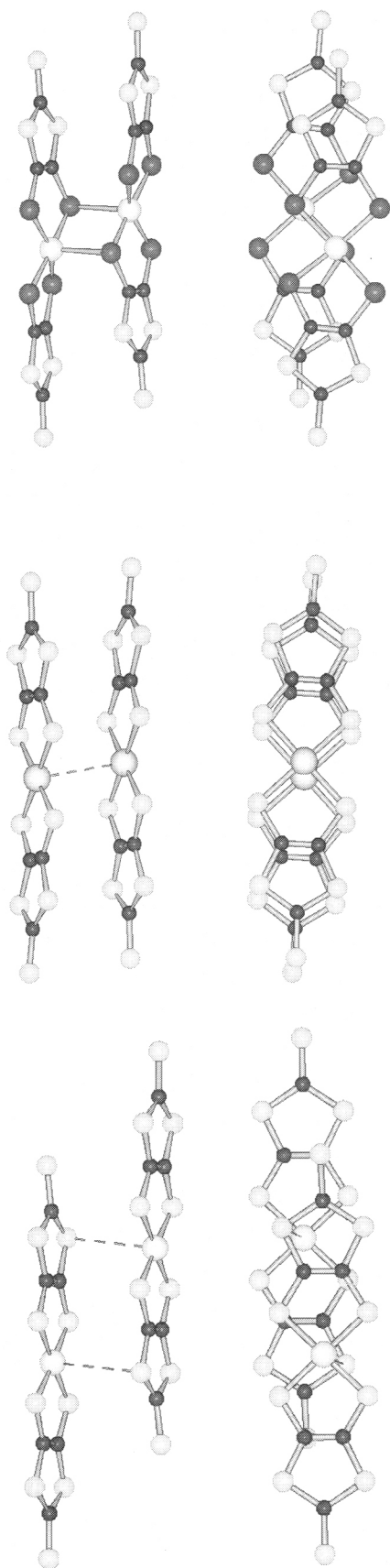
Fig. 1.18. The dimer arrangements and dimer overlapping are illustrated for [Fe(Cp*)₂][Ni(dmit)₂] (top) and α-[Fe(Cp*)₂][Pd(dmit)₂] (center) and [Fe(Cp*)₂][Ni(dsit)₂] (bottom).

1.3.4   Type IV Mixed Chain [M(Cp*)₂][M′(L)₂] Salts

The magnetic behavior of the [M(Cp*)₂][M′(L)₂] salts based on type IV chains shows a strong dependence on the intra and interchain arrangments. Table 1.5 summarizes the key magnetic properties of type IV [M(Cp*)₂][M′(L)₂] compounds.

Table 1.5. Magnetic characterization of type IV [M(Cp*)₂][M′(L)₂] salts.

Compound	S_D; S_A	θ, K	Comments	Ref.
[Fe(Cp*)₂][Ni(dmio)₂]MeCN	1/2; 1/2	2.0	(a)	32
[Fe(Cp*)₂][Ni(bds)₂]MeCN	1/2; 1/2	0 (b)	(a)	17
[Fe(Cp*)₂][Ni(bdt)₂]	1; 1/2	−5.6 (c)	(a); T_m = 40 K (d)	33, 48
[Mn(Cp*)₂][Ni(bdt)₂]	1; 1/2	−22.6	T_m = 20 K (d); MM (e): T_N = 2.3 K; H_C = 200 G (2 K)	33, 48
[Cr(Cp*)₂][Ni(bdt)₂]	3/2; 1/2	+6.2	(a)	33, 48
[Fe(Cp*)₂][Co(bdt)₂] (f)	3/2; 1	−23.0	(a)	33
[Mn(Cp*)₂][Co(bdt)₂] (f)	3/2; 1	−4.9	(a)	33
[Cr(Cp*)₂][Co(bdt)₂]	3/2; 1	−2.5	(a)	33
[Fe(Cp*)₂][Pt(bdt)₂]	1/2; 1/2	−12.6	(a); T_m = 125 K (d)	33
[Mn(Cp*)₂][Pt(bdt)₂] (f)	1; 1/2	−20.5	T_m = 100 K (d); FIM (g): T_C = 2.7 K	33
[Cr(Cp*)₂][Pt(bdt)₂]	3/2; 1/2	+6.0	(a)	33
[Fe(Cp*)₂]₂[Cu(mnt)₂]	1/2; 1/2	−8.0	(a)	29

(a) No magnetic ordering observed down to 1.8 K. (b) θ value in the high temperature region, at low temperatures $\theta > 0$. (c) Non-Curie–Weiss behavior the given θ value relates to the high temperature region ($T > T_m$). (d) Minimum in χT vs. T. (e) Metamagnetic transition. (f) Crystal structure not yet determined. (g) Ferrimagnetic transition.

1.3.4.1   [Fe(Cp*)₂][Ni(dmio)₂]MeCN

The crystal structure of [Fe(Cp*)₂][Ni(dmio)₂]MeCN consists of 2D layers composed of parallel ··D⁺D⁺A⁻D⁺D⁺A⁻·· chains (type IV), where side-by-side pairs of donors alternate with an acceptor, with a net charge (+) per repeat unit (D⁺D⁺A⁻) [32]. These charged layers are separated by acceptor layers, as represented in the view along [010] in Figure 1.19, for [Fe(Cp*)₂][Ni(dmio)₂]MeCN. The chains are regular and the Cp fragments of the donor sit above the dmio ligands of the acceptor, as shown in Figure 1.19(a). In this compound, unlike the previous compounds, the C₅Me₅ ligands from [Fe(Cp*)₂]⁺ present an eclipsed conformation. No interionic short contacts are observed in [Fe(Cp*)₂][Ni(dmio)₂]MeCN. The closest interionic intrachain (DA) separation involves a S atom from the central
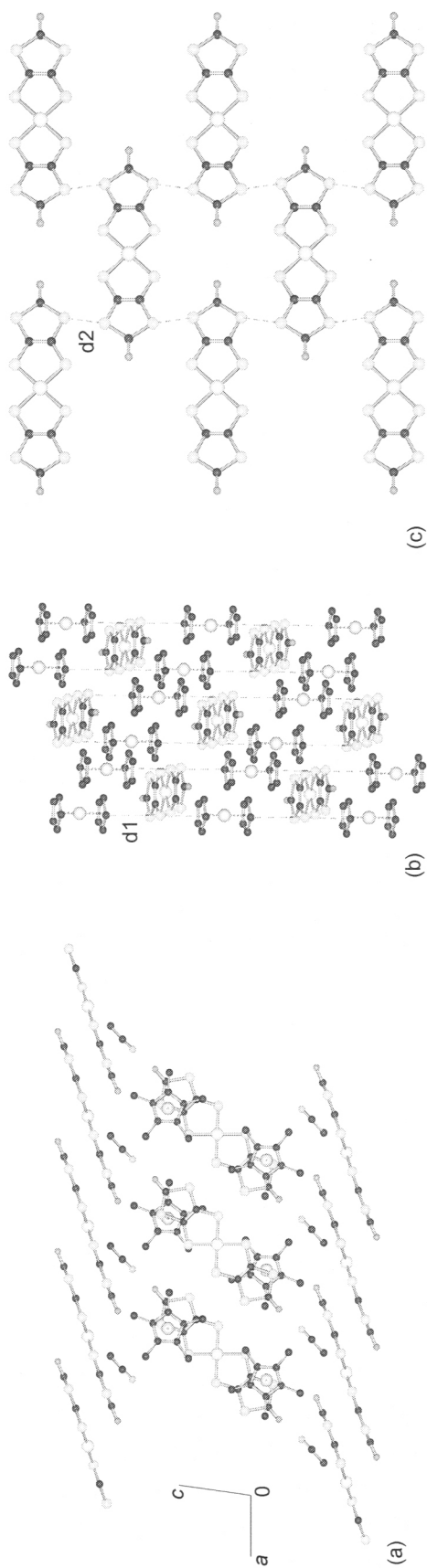
Fig. 1.19. (a) View of the crystal structure of $[Fe(Cp^*)_2]|[Ni(dmio)_2]MeCN$ along the stacking direction (hydrogen atoms were omitted for clarity). (b) View of the DDA layer, d1 corresponds to the intrachain (DA) closest contacts (3.945 Å, $Q_W = 1.14$) (Me groups were omitted for clarity). (c) View of the anionic layer, d2 is the closest interlayer contact (3.777 Å, $Q_W = 1.02$).

MS_4 fragment of the acceptor and one of the C atoms from the C5 ring of the donor, with a S–C distance of 3.945 Å ($Q_W = 1.14$). The chains in the layers are quite isolated and the solvent molecules are located in cavities between the DDA chains layers and the anionic layers, as shown in the view of the structure in Figure 1.19(b). Short contacts were observed in the anionic layers involving S atoms from the five-membered C_2S_2C ring of the dmio ligands, with a S–S distance of 3.777 Å ($Q_W = 1.02$), as shown in Figure 1.19(c). Relatively close AA contacts between the DDA chains and the anionic layers were also observed in $[Fe(Cp^*)_2][Ni(dmio)_2]$, involving O atoms from the acceptor layers and S atoms from the C_2S_2C ring of the dmio ligands, with a O–S distance of 3.398 Å ($Q_W = 1.05$).

In the case of $[Fe(Cp^*)_2][Ni(dmio)_2]MeCN$, FM interactions dominate the magnetic behavior of the compounds [32], as seen from the positive θ value (2 K) obtained from the Curie–Weiss fit. The observed magnetic behavior is attributed to the intrachain interactions, as the contacts in the anionic layers are expected to give rise to AFM interactions since the spin density of the atoms involved in these contacts have the same sign.
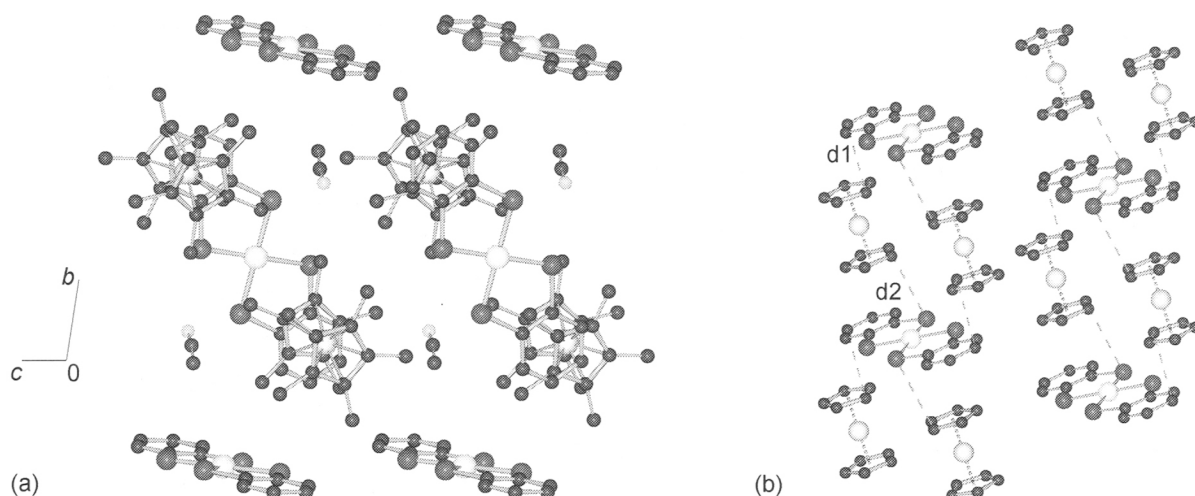
1.3.4.2 $[Fe(Cp^*)_2][Ni(bds)_2]MeCN$

The crystal structure of $[Fe(Cp^*)_2][Ni(bds)_2]$, as that of $[Fe(Cp^*)_2][Ni(dmio)_2]MeCN$, consists of 2D layers composed of parallel $··D^+D^+A^-D^+D^+A^-··$ chains (type IV), which are separated by acceptor layers [17], as represented in the view along [100] in Figure 1.20(a). In the case of $[Fe(Cp^*)_2][Ni(bds)_2]MeCN$, the chains are not regular and while one of the Cp fragments of the donor sits above the C6 ring of the ligand, the second is displaced towards the center of the acceptor. For the first Cp the closest DA interatomic separation (C–C) has a distance of 3.451 Å ($Q_W = 1.08$), while for the second Cp the closest DA contact (C–Se) corresponds to a distance of 3.752 Å ($Q_W = 1.04$), as shown in Figure 1.20(b). The DDA chains are relatively isolated and the solvent is located in cavities between the chains. In the case of $[Fe(Cp^*)_2][Ni(bds)_2]MeCN$ no short interionic interlayer distances were observed involving molecules in the DDA layers, not in acceptor layers or even in the anionic layers.

The magnetic behavior of this compound is dominated by FM interactions [17], which are attributed to the observed DA intrachain contacts.

1.3.4.3 $[M(Cp^*)_2][M'(bdt)_2]$ (M = Fe, Mn and Cr; M' = Co, Ni and Pt)

$[Cr(Cp^*)_2][M'(bdt)_2]$ (M' = Ni and Co) are isostructural, and, as in the case of the $[Fe(Cp^*)_2][Ni(dmio)_2]MeCN$ and $[Fe(Cp^*)_2][Ni(bds)_2]MeCN$ salts, a crystal structure, based on a DDA type IV chain supramolecular arrangement, is observed [33]. However in $[Cr(Cp^*)_2][M'(bdt)_2]$ the pairs of donors are perpendicular to each other, unlike the previous compounds, where the donor molecules are
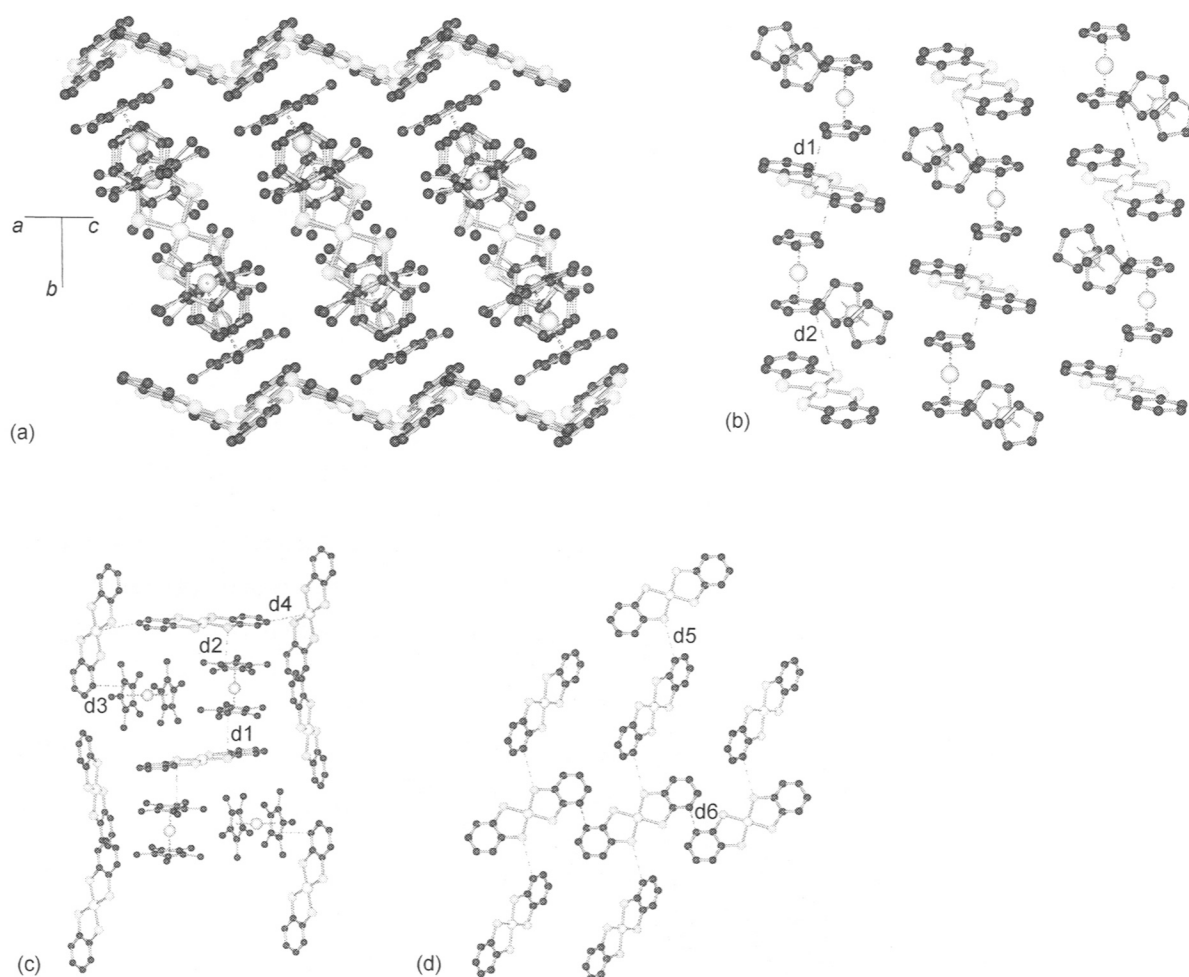
Fig. 1.20. (a) Perspective view of the crystal structure of [Fe(Cp*)$_2$][Ni(bds)$_2$]MeCN normal to the chain direction (hydrogen atoms were omitted for clarity). (b) View of the DDA layer, d1 and d2 correspond to the intrachain (DA) closest contacts (3.451 and 3.752 Å, $Q_W = 1.08$ and 1.04) (Me groups were omitted for clarity).

parallel. A view along the chain direction, [101], is shown in Figure 1.21(a) for [Cr(Cp*)$_2$][Ni(bdt)$_2$]. The shorter DA intrachain separations involve S atoms from the acceptors and C atoms from the Cp rings of the donors (aligned with the chain direction) presenting S–C distances of 3.702 and 3.857 Å ($Q_W = 1.07$ and 1.12), as shown in the view of a DDA chain layer represented in Figure 1.21(b). The chains in the same layer are relatively isolated, but short distances between the chains and anions on the anionic layers were observed. As shown in Figure 1.21(c), besides the intrachain contacts, relatively short interaionic separations were also observed between molecules in the chains and in the anionic layers. AA contacts were observed involving C atoms from the terminal C6 ring of the ligands and Ni atoms from the acceptors in the anionic layer, with a C–Ni distance of 4.206 Å ($Q_W = 1.14$). DA contacts were also observed involving one of the C atoms from the Cp ring of the donor perpendicular to the chain axis and one of the C atoms from the C6 ring of the acceptor, with a C–C distance of 3.453 Å ($Q_W = 1.08$). Short contacts were also observed in the anionic layers, as shown in Figure 1.21(d), with distances of 3.633 and 3.340 Å ($Q_W = 1.05$ and 1.04), for S–C and C–C contacts respectively. In the case of [Fe(Cp*)$_2$][M'(bdt)$_2$] (M' = Ni and Pt), [Mn(Cp*)$_2$][M(bdt)$_2$] (M' = Ni and Co), and [Cr(Cp*)$_2$][Pt(bdt)$_2$], the crystal structures show a duplication of the unit cell along b, but present similar supramolecular packing [33].

In the case of the compounds [M(Cp*)$_2$][Co(bdt)$_2$] (M = Fe, Mn and Cr) and [Cr(Cp*)$_2$][M'(bdt)$_2$] (M' = Ni and Pt), the magnetic susceptibility follows Curie–Weiss behavior. The [M(Cp*)$_2$][Co(bdt)$_2$] salts present dominant AFM interactions ($\theta = -23$, -4.9 and -2.5 K for M = Fe, Mn and Cr respectively) [33], while the [Cr(Cp*)$_2$][M'(bdt)$_2$] present dominant FM interactions ($\theta = 6.2$ and 6.0 K for M' = Ni and Pt respectively) [33]. In the case of the compounds [Fe(Cp*)$_2$][M'(bdt)$_2$] and [Mn(Cp*)$_2$][M'(bdt)$_2$], with M' = Ni and Pt, a minimum in the temperature

Fig. 1.21. (a) View of the crystal structure of $[Fe(Cp^*)_2][Pt(bdt)_2]$ along the chain direction (hydrogen atoms were omitted for clarity). (b) View of the DDA layer, d1 and d2 correspond to the intrachain (DA) closest contacts (3.702 and 3.857 Å, $Q_W = 1.07$ and 1.12) (Me groups were omitted for clarity). (c) View of one of the DDA stacks and acceptors from neighboring acceptor layers, d3 and d4 correspond to interlayer contacts (3.453 and 4.206 Å, $Q_W = 1.08$ and 1.14). (d) View of the anionic layer, d5 (S–C) and d6 (C–C) are the closest interlayer contacts (3.633 and 3.340 Å, $Q_W = 1.05$ and 1.04).

dependence of χT is observed at 40, 125, 20 and 130 K for M/M' = Fe/Ni, Fe/Pt, Mn/Ni and Mn/Pt respectively [33]. For these compounds the minima are attributed to ferrimagnetic behavior, as in the case of $[Mn(Cp^*)_2][Pt(bdt)_2]$ FIM ordering was observed at 2.7 K [33]. The magnetization field dependence, at 1.8 K, is shown in Figure 1.22 (squares), after a fast increase at low fields the magnetization attains an almost constant value that is in good agreement with that predicted for FIM ordering, $M_{sat} = S_D g_D - S_A g_A \approx 1.57 N \mu_B$, calculated for $S_A = 1/2$, $g_A = 2.06$ [49], $S_D = 1$ and $g_D = 2.6$ (due to the high g anisotropy of the donor the g_D value was obtained from susceptibility temperature dependence at high temperatures). The magnetization field dependence, at 2 K, of $[Mn(Cp^*)_2][Ni(bdt)_2]$ is also shown in Figure 1.22 (circles). A metamagnetic transition was observed to occur in this compound, with $T_N = 2.3$ K and $H_C = 200$ G at 2 K [33, 48], as
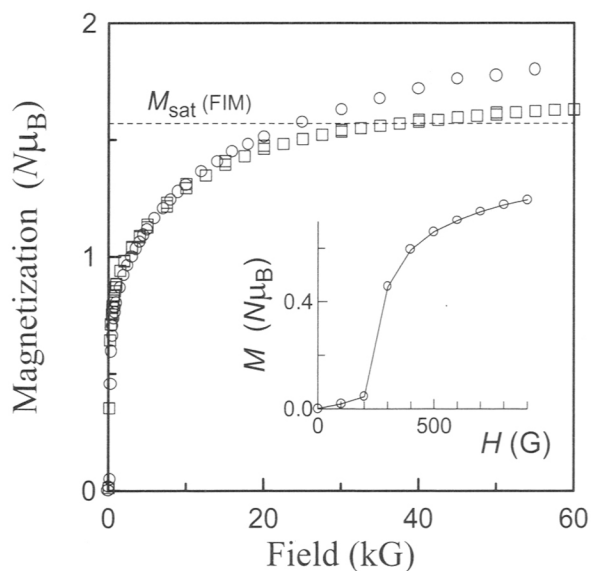
**Fig. 1.22.** Magnetization field dependence for [Mn(Cp*)$_2$][Pt(bdt)$_2$] (squares) and [Fe(Cp*)$_2$][Ni(bdt)$_2$] (circles) at 1.8 K. The inset shows the low field sigmoidal behavior observed in the case of [Fe(Cp*)$_2$][Ni(bdt)$_2$].

shown in the inset of Figure 1.22. The magnetization values above the critical field, in the high field state, are of the same order as those observed in the case of [Mn(Cp*)$_2$][Pt(bdt)$_2$] and are considerably inferior than the FM saturation magnetization value, $M_{sat} = S_D g_D + S_A g_A \approx 3.53\,N\,\mu_B$, calculated for $S_A = 1/2$, $g_A = 2.06$ [49], $S_D = 1$ and $g_D = 2.5$ (the g_D value was obtained from the susceptibility temperature dependence at high temperature). Then the high field state of [Mn(Cp*)$_2$][Ni(bdt)$_2$] is consistent with a FIM state. The complexity of the crystal structure of the [M(Cp*)$_2$][M'(bdt)$_2$] salts prevents clear interpretation of the magnetic behavior and the discussion of the correlation between the crystal structures and the magnetic properties.

1.3.4.4   [Fe(Cp*)$_2$]$_2$[Cu(mnt)$_2$]

[Fe(Cp*)$_2$]$_2$[Cu(mnt)$_2$] presents a crystal structure based on an arrangement of DDA type IV chains. Unlike the other compounds based on these types of chains in [Fe(Cp*)$_2$]$_2$[Cu(mnt)$_2$] the chains are neutral, as the acceptor is a dianion, [Cu(mnt)$_2$]$^{2-}$, and there are no anionic layers in this compound [29]. A view along the chain direction, [101], is shown in Figure 1.23(a) for [Fe(Cp*)$_2$]$_2$[Cu(mnt)$_2$]. In this compound both donors, from the DD pair in the repeat unit, are perpendicular to the chain direction, as shown in Figure 1.23(b). Short intrachain contacts were observed and involve the Cu from the acceptor and a C from one of the Me groups in the donor, with a Cu–C distance of 3.562 Å ($Q_W = 0.96$). The side-by side donors are relatively close and C–C distances of 3.826 Å ($Q_W = 1.20$) were observed, involving C atoms from the Cp fragments. No short interionic intrachain contacts were observed and the chains are essentially isolated.

For [Fe(Cp*)$_2$]$_2$[Cu(mnt)$_2$] the magnetic susceptibility follows Curie–Weiss behavior, with $\theta = -7.95$ K [29]. The dominant antiferromagnetic interactions observed for this compound are consistent with the type of contacts, C–S (DA) or
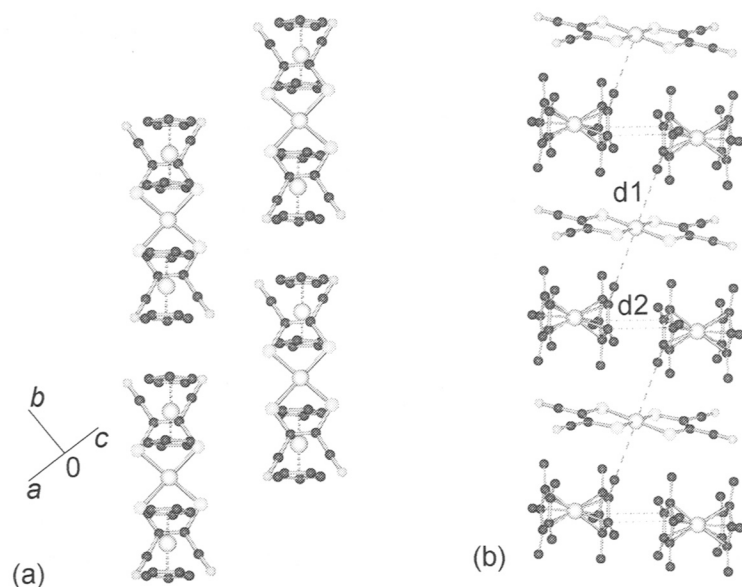
Fig. 1.23. (a) Perspective view of the crystal structure of $[Fe(Cp^*)_2]_2[Cu(mnt)_2]$ along the chain direction. (b) View of one of the DDA chains, where d1 is the closest interionic contact (3.562 Å, $Q_W = 1.05$), relatively short DD separations (d2 = 3.826 Å, $Q_W = 1.20$) were detected. Hydrogen atoms were omitted for clarity.

C–C (DD), observed in the crystal structure, as the spin density is expected to be of the same sign in the atoms involved in the contacts.

1.3.5 Salts with Segregated Stacks not 1D Structures

Most of the ET salts based on decamethylmetallocenium radical donors and on planar metal dichalcogenide radical anions reported so far present crystal structures with mixed linear chain basic motifs. The only known exception is $[Fe(Cp^*)_2][Ni(mnt)_2]$, which exhibits a non-1D crystal structure based on a $D^+[A_2]^{2-}D^+$ repeat unit [16]. In the case of this compound the magnetic behavior is dominated by intradimer antiferromagnetic interactions.

As most of the work with this type of ET salts was essentially motivated by the results obtained with the salts based on decamethylmetalocenium donors and polynitrile planar acceptors, the use of different metallocenium derivatives was limited to a small number of compounds. Among these only the $[Fe(C_5Me_4SCMe_3)_2][M(mnt)_2]$, M = Ni and Pt, which was described previously, presented crystal structures based on mixed linear chain motifs. The work developed with salts of other metallocenium derivative donors, including also diamagnetic donors, was also motivated by the observation of ferromagnetic ordering in $NH_4[Ni(mnt)_2]H_2O$ [7], as the magnetic ordering in this compound is only due to the acceptors. At room temperature, the crystal structure of this salt consists of regular stacks of eclipsed acceptors and the magnetic behavior of $NH_4[Ni(mnt)_2]H_2O$ is dominated by AFM interactions down to ca. 100 K, where a structural transition

occurs, below this temperature FM interactions become dominant, and magnetic ordering occurs at 4.5 K.

In the case of the salts with $[M(mnt)_2)]^-$ (M = Ni and Pt) acceptors, the anionic stacks are isolated from each other by the cations and within the stacks the $[M(mnt)_2)]^-$ units form dimers. The magnetic behavior of these compounds is dominated by AFM interactions between the acceptor units in the dimers.

1.4 Summary and Conclusions

In this chapter we have reviewed the study of ET salts based on metallocenium radical donors and on planar metal bis-dichalcogenate radical anions. The crystal structures (all molecular and crystal structure representations were performed using SCHAKAL-97 [50]) of these salts were correlated with the magnetic properties, and the magnetic coupling was analyzed in the perspective of the McConnell I mechanism.

The use of the planar metal bis-dichalcogenate acceptors in the preparation of new molecule-based materials followed the report of bulk ferromagnetism in decamethylmetallocenium-based ET salts with small polynitrile acceptors such as TCNE and TCNQ. One of the goals related to the use of the metal bis-dichalcogenate acceptors is to obtain an increase in the dimensionality in relation to polynitrile-based ET salts and, as a consequence, to obtain new materials with interesting cooperative magnetic properties. A large number of new ET salts have been obtained, presenting a variety of molecular arrangements, which depend essentially on the size of the anionic complexes, on the tendency of the acceptors to associate as dimers and also on the extent of the π system in the ligands. These salts exhibit a large variety of magnetic behavior. Different types of magnetic ordering were observed at low temperatures.

ET salts with small acceptors such as $[M(edt)_2]^-$, $[M(tdt)_2]^-$ and $[M(tds)_2]^-$ (M = Ni, Pd, Pt), where the delocalized electrons are confined to the central $M(S_2C_2)_2$ fragment, present crystal structures based on parallel arrangements of alternated DADA chains, and in several of these compounds metamagnetic behavior was observed, in good agreement with the predictions of the McConnell I mechanism.

In ET salts based on anionic complexes with a large extent of the π system of the ligands two types of structures were observed, depending on the tendency of the complexes to form dimers. In the cases of $[M(dmit)_2]^-$ and $[M(dmio)_2]^-$, which show a strong tendency to dimerize, in most cases the crystal structure consists of an arrangement of 2D layers composed of parallel chains, where face-to-face pairs of acceptors alternate with side-by-side pairs of donors, DDAA. The magnetic behavior of these ET salts is strongly dependent on the AA interactions, where a competition between FM and AFM interactions is expected. AFM dominant inter-

actions were observed at high temperatures, in good agreement with the McConnell I mechanism predictions. In the case of $[M(Cp^*)_2][Ni(dmit)_2]$ (M = Fe and Mn) at low temperatures FM becomes dominant and in the case of $[Mn(Cp^*)_2][Ni(dmit)_2]$ a FM transition occurs at 2.5 K, this is attributed to a change in the type of the dominant magnetic interactions.

In the case of the ET salts based on anionic complexes presenting a large extent of the π system but no tendency to exist as dimers, such as $[Ni(bds)_2]^-$, $[M(bdt)_2]^-$ (M = Co, Ni and Pt), and $[Cu(mnt)_2]^{2-}$, in general the crystal structures are based on 2D layers consisting of parallel chains where acceptors alternate with pairs of donors, ADDADD, and these layers are separated by layers of acceptors. In these compounds the relative orientation of the donor pairs depends on the acceptors. In the case of $[Fe(Cp^*)_2][Ni(bds)_2]$ the donors are parallel and with their axes roughly aligned along the stacking direction, for $[Fe(Cp^*)_2]_2[Cu(mnt)_2]$ the donors are also parallel but their axes are perpendicular to the stacking direction, while for the $[M(Cp^*)_2][M'(bdt)_2]$ salts the donors from the pairs are perpendicular, one is aligned with the stacking direction and the other is perpendicular to it. While for $[Fe(Cp^*)_2][Ni(bds)_2]$ and $[Fe(Cp^*)_2]_2[Cu(mnt)_2]$ the magnetic behavior is dominated by the intrachain DA magnetic interactions, which were observed to be FM and AFM respectively. In the case of the $[M(Cp^*)_2][M'(bdt)_2]$ compounds, a large number of contacts were observed in the relatively complex structure, and a variety of magnetic behaviors was observed.

In spite of the simplicity of McConnell I model, it has shown to be quite effective in the interpretation of the magnetic behavior in the ET salts based on metallocenium radical donors and on planar metal bis-dichalcogenate radical anions. However in the compounds presenting complex structures with possible competition between FM and AFM intermolecular contacts, e. g. the compounds $[M(Cp^*)_2][Ni(\alpha\text{-tpdt})_2]$, $[M(Cp^*)_2][M'(dmit)_2]$ and $[M(Cp^*)_2][M'(bdt)_2]$, it was not possible to achieve a clear understanding of the magnetic behavior with that model.

The study of these type of ET salts, which began in the late 80s, has gained renewed interest in recent years and a large number of compounds are still under study. Besides the significant number of compounds presenting metamagnetism, the use of acceptors showing spin polarization, leads to salts presenting other types of ordering, such as ferro and ferrimagnetism. The use of these types of acceptors seems quite promising for the preparation of new molecule-based materials.

Acknowledgments

References

1. A. Kobayashi, H. Kobayashi, in *Handbook of Organic Conductive Molecules and Polymers*, ed. H.S. Nalwa, John Wiley, Chichester, **1997**, Vol. 1, p. 249.
2. A. Kobayashi, H. Kim, Y. Sasaki et al., *Chem. Lett.* **1987**, 1819.
3. J.W. Bray, H.R. Hart, Jr., L.V. Interrante et al., *Phys. Rev. Lett.* **1975**, *35*, 744.
4. M. Almeida, R.T. Henriques, in *Handbook of Organic Conductive Molecules and Polymers*, ed. H.S. Nalwa, John Wiley, Chichester, **1997**, Vol. 1, p. 87.
5. C. Rovira, J. Veciana, E. Ribera et al., *Angew. Chem. Int. Ed. Engl.*, **1997**, *36*, 2323.
6. J.P. Sutter, M. Fettouhi, C. Michaut et al., *Angew. Chem. Int. Ed. Engl.*, **1996**, *35*, 2113.
7. M.L. Allan, A.T. Coomber, I.R. Marsden et al., *Synth. Met.*, **1993**, *55-57*, 3317.
8. J.S. Miller, J.C. Callabrese, H. Rommelmann et al. *J. Am. Chem. Soc.*, **1987**, *109*, 769.
9. S. Chittipedi, K.R. Cromack, J.S. Miller et al., *Phys. Rev. Lett.*, **1987**, *58*, 2695.
10. J.S. Miller, A.J. Epstein, in *Research Frontiers in Magnetochemistry*, ed. C. J. O'Connor, World Scientific, Singapore, 1993, p. 283.
11. J.S. Miller, A.J. Epstein, in E. Coronado, P. Delhaès, D. Gatteschi, J.S. Miller (ed.) *Molecular Magnetism: From Molecular Assemblies to Devices*, ed. E. Coranado, P. Delhaès, D Gatteschi et al., Kluwer, Dordrecht, 1996, p. 379.
12. (a) G.T. Yee, J.M. Manriquez, D.A. Dixon et al., *Adv. Mater.* **1991**, *3*, 309; (b) D.M. Eichhorn, D.C. Skee, W.E. Broderick et al., *Inorg. Chem.* **1993**, *32*, 491; (c) J.S. Miller, R.S. McLean, C. Vasquez et al., *J. Mater. Chem.* **1993**, *3*, 215.
13. (a) W.E. Broderick, D.M. Eichhorn, X. Liu et al., *J. Am. Chem. Soc.* **1995**, *117*, 3641; (b) W.E. Broderick, J.A. Thompson, E.P. Day et al., *Science* **1990**, *249*, 401; (c) W.E. Broderick, B.M. Hoffman, *J. Am. Chem. Soc.* **1991**, *113*, 6334.
14. O. Kahn, *Molecular Magnetism*, VCH, New York, **1993**, Chapter 11.
15. J.S. Miller, A.J. Epstein, *Angew. Chem. Int. Ed. Engl.* **1994**, *33*, 385.
16. J.S. Miller, J.C. Calabrese, A.J. Epstein, *Inorg. Chem.* **1989**, *28*, 4230.
17. W.E. Broderick, J.A. Thompson, M.R. Godfrey et al., *J. Am. Chem. Soc.* **1989**, *111*, 7656.
18. H.M. McConnell, *J. Chem. Phys.* **1963**, *39*, 1910.
19. H.M. McConnell, *Proc. Robert A. Welch Found. Conf. Chem. Res.* **1967**, *11*, 144.
20. O. Kahn, *Molecular Magnetism*, VCH, New York, **1993**, Chapter 12.
21. M. Deumal, J. J. Novoa, M. J. Bearpark et al., *J. Phys, Chem. A* **1998**, *102*, 8404.
22. M. Deumal, J. Cirujeda, J. Veciana et al., *Chem. Eur. J.* **1999**, *5*, 1631.
23. V. Gama, D. Belo, S. Rabaça et al., *Eur. J. Inorg. Chem.* **2000**, *9*, 2101.
24. W.E. Broderick, J.A. Thompson, B.H. Hoffman, *Inorg. Chem.* **1991**, *30*, 2960.
25. J.S. Miller, personal communication.
26. S. Rabaça, R. Meira, L.C.J. Pereira et al., *Inorg. Chim. Acta.* **2001**, *326*, 89.
27. S. Rabaça, R. Meira, V. Gama et al., *Acta Crystallogr., Sect. C.*, submitted.
28. S. Rabaça, R. Meira, L.C.J. Pereira et al., manuscript in preparation.
29. M. Fettouhi, L. Ouahab, M. Hagiwara et al., *Inorg. Chem.* **1995**, *34*, 4152.
30. (a) C. Faulmann, personal communication; (b) Communication in the *4th International Symposium on Crystalline Organic Metals, Superconductors and Ferromagnets (ISCOM2001)*, Hokkaido, Japan, September 10–14, 2001 (p. 127 in the Book of Abstracts).
31. S. Rabaça, M.T. Duarte, V. Gama, manuscript in preparation.
32. M. Fettouhi, L. Ouahab, E. Codjovi et al., *Mol. Cryst. Liq. Cryst.* **1995**, *273*, 29.
33. S. Rabaça, D. Belo, H. Alves et al., manuscript in preparation.

34. D. Belo, H. Alves, S. Rabaça et al., *Eur. .J. Inorg. Chem.* **2001**, *12*, 3127.

35. D. Belo, J. Mendonça, R. Meira et al., manuscript in preparation.

36. S. Zürcher, V. Gramlich, D. Arx, A. Togni, *Inorg. Chem.* **1998**, *37*, 4015.

37. S. Alvarez, R. Vicente, R. Hoffmann, *J. Am. Chem. Soc.* **1985**, *107*, 6253.

38. M. Sano, H. Adachi, H. Yamatera, *Bull. Chem. Soc. Jpn.* **1981**, *54*, 2636.

39. M.W. Day, J. Qin, C. Yang, *Acta Crystallogr., Sect. C* **1998**, *54*, 1413.

40. M. Hobi, S. Zürcher, V. Gramlich et al., *Organometallics* **1996**, *15*, 5342.

41. A. Pullen, C. Faulmann, K.I. Pokhodnya et al., *Inorg. Chem.* **1998**, *37*, 6714.

42. F. Qi, Y. Xiao-Zeng, C. Jin-Hua et al., *Acta Crystallogr., Sect. C* **1993**, *49*, 1347.

43. C. Faulmann, F. Delpech, I. Malfant et al., *J. Chem. Soc., Dalton Trans.* **1996**, 2261.

44. V. Gama, S. Rabaça, C. Ramos et al., *Mol. Cryst. Liq. Cryst.* **1999**, *335*, 81.

45. S. Rabaça, V. Gama, D. Belo et al., *Synthetic Met.* **1999**, *103*, 2303.

46. C. Faulmann, A.E. Pullen, E. Rivière et al., *Synthetic Met.* **1999**, *103*, 2296.

47. Y. Journaux, Communication in the *6th FIGIPS Meeting on Inorganic Chemistry*, Barcelona, Spain, July 15–20, 2001 (p. 49 in the Book of Abstracts).

48. V. Gama, D. Belo, I.C. Santos et al., *Mol. Cryst. Liq. Cryst.* **1997**, *306*, 17.

49. J.A. McCleverty, *Progress in Inorganic Chemistry*, Vol. 10, ed. by F.A. Cotton, Interscience, New York, 1968, p. 49.

50. E. Keller, *SCHAKAL-97, A Computer Program for the Graphical Representation of Molecular and Crystallographic Models*, Krystallographisches Institut der Universitat Freiburg, Germany, **1997**.